Computer-Integrated Surgical System

November 11th, 2009

Mamoru Mitsuishi
Department of Mechanical Engineering
School of Engineering
The University of Tokyo

Medical Robots M.Mitsuishi, The University of Tokyo

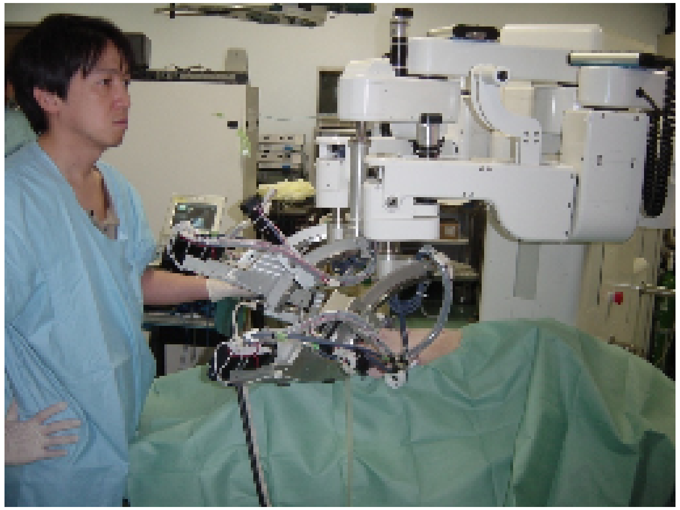

△ Remote minimally invasive surgical system

△ Bone cutting robot for total knee arthroplasty (TKA)

△ Robot to assist femur fracture reduction

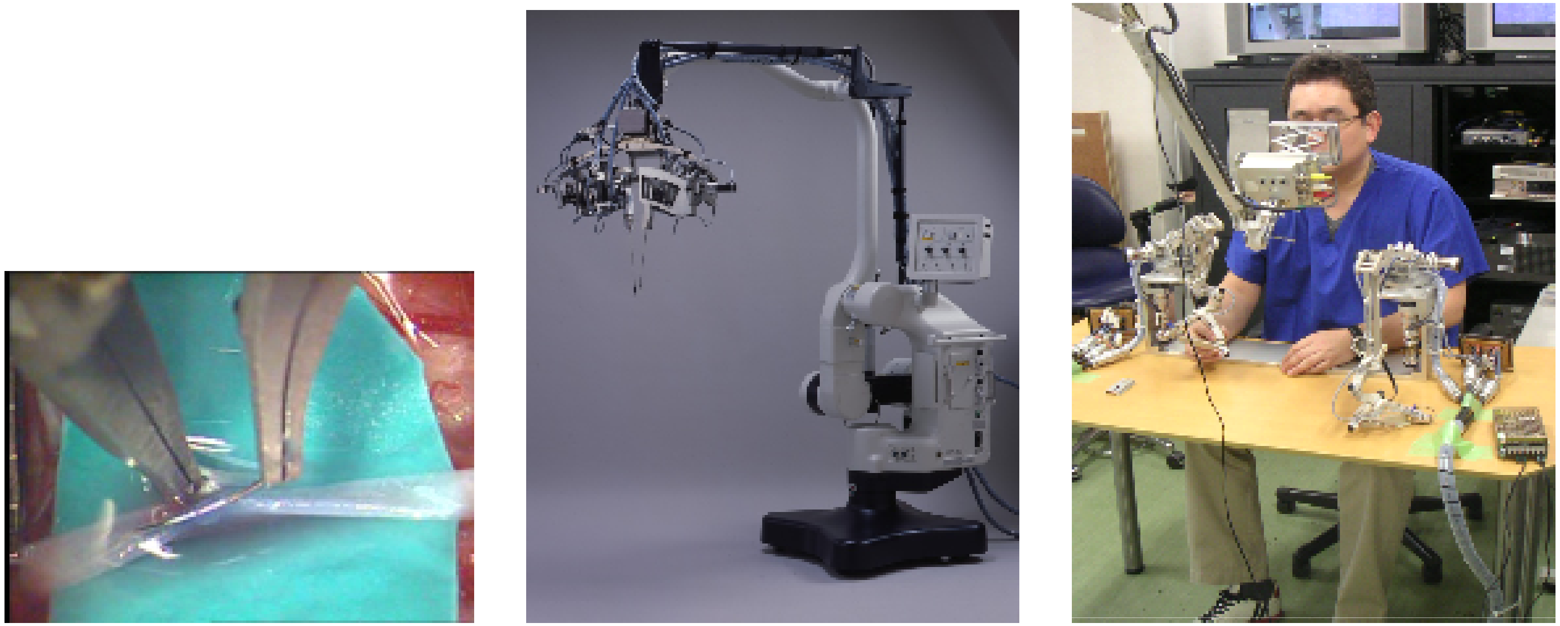

△ Neurosurgery system in the deep surgical field

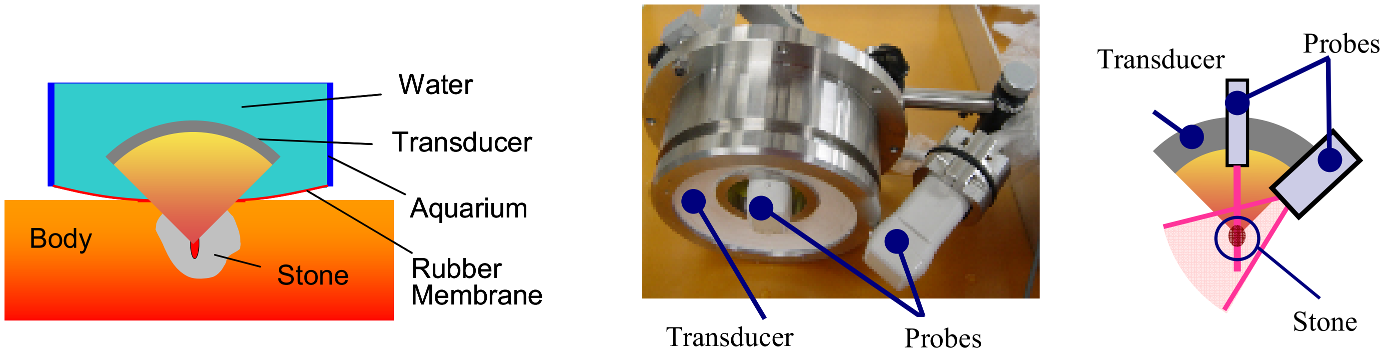

△ Noninvasive ultrasound therapy system

To realize a computer-integrated surgical system …

1. Image processing and presentation
2. Modeling and segmentation
3. Registration and navigation
4. Mechanism
5. Tele-care/tele-surgery and macro-micro tele-operation

Contents

Current state and future direction of the computer-integrated surgical system

2000 | 2007 | 2025 | 2050

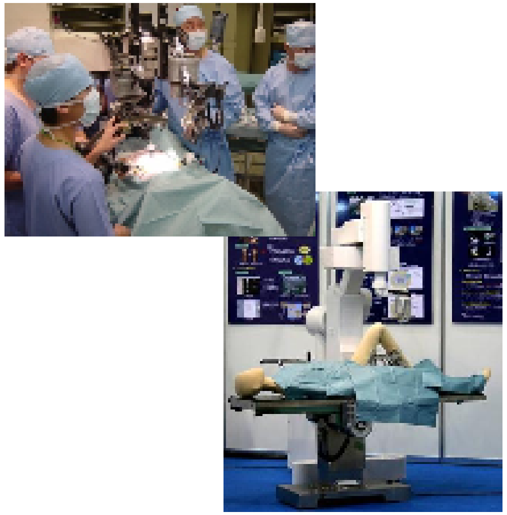

Current technology

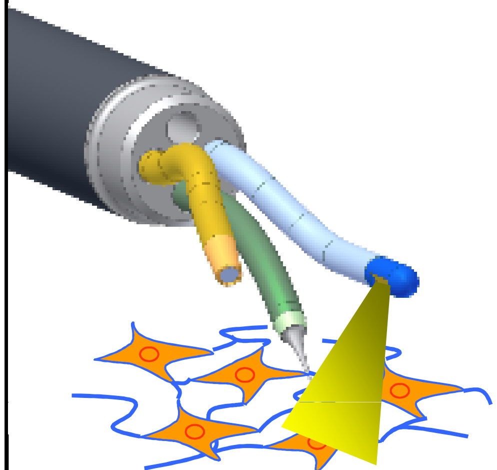

Technology in 2025

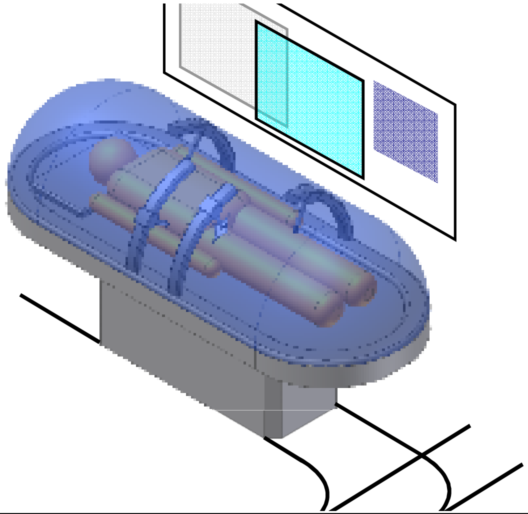

Technology in 2050

Current technology

- X-ray, CT, MRI (static image) (resolution: 0.1 mm)
- Endoscope (diameter: 10 mm)
- Forceps (diameter: 10 mm)
- Organ level therapy (mm order)
- Diagnosis and treatment are executed by a surgeon

Technology in 2025

- Imaging in the body (micro meter order)
- Real-time continuous imaging of the motion and the deformation for an internal organ and a heart (4D)
- Local and high precision non- and minimally-invasive cell level target therapy (micro meter order)
- Integration of diagnosis and treatment

Technology in 2050

- Shape analysis to function analysis for imaging
- Capsule type diagnostic and treatment environment to keep clean, high oxygen density, low temperature and high pressure around the patient
- From surgical operation to dosage, regeneration, diagnosis and prophylaxis using tissue engineering (organ/vessel, bone, skin and nerve), nano diagnosis and treatment (nano immunity diagnosis, gene therapy and DDS)
- Automatic diagnosis and treatment (pathological diagnosis using medical image. Treatment is executed automatically.)

Background

Arthroplasty

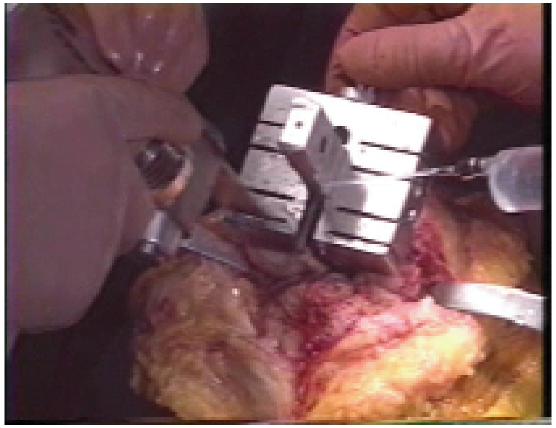

MIS

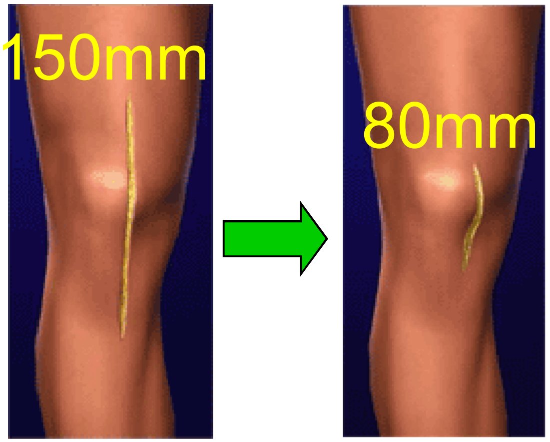

Conventional MIS

Necessity of computer-integrated surgery

(1) Small incision increases the difficulty

(2) Increase of error for implant position and posture

Computer-integrated surgery for MIS arthroplasty

Requirements for minimally invasive orthopedic surgery

Less invasiveness

- Small incision: ***less than 100 mm***
- Less invasiveness to the soft tissue and the bone

Safety

- No damage to the surrounding tissues
- No tool breakage

Precision

- Shape accuracy of the setting plane for the artificial joint: ***angle error: less than 2 deg., position error: less than 2 mm***
- Difficulty of the cutting tool approach

Efficiency

- Operation time for ***bone cutting is limited within 15 minutes.***

Expectation for a robotic surgery

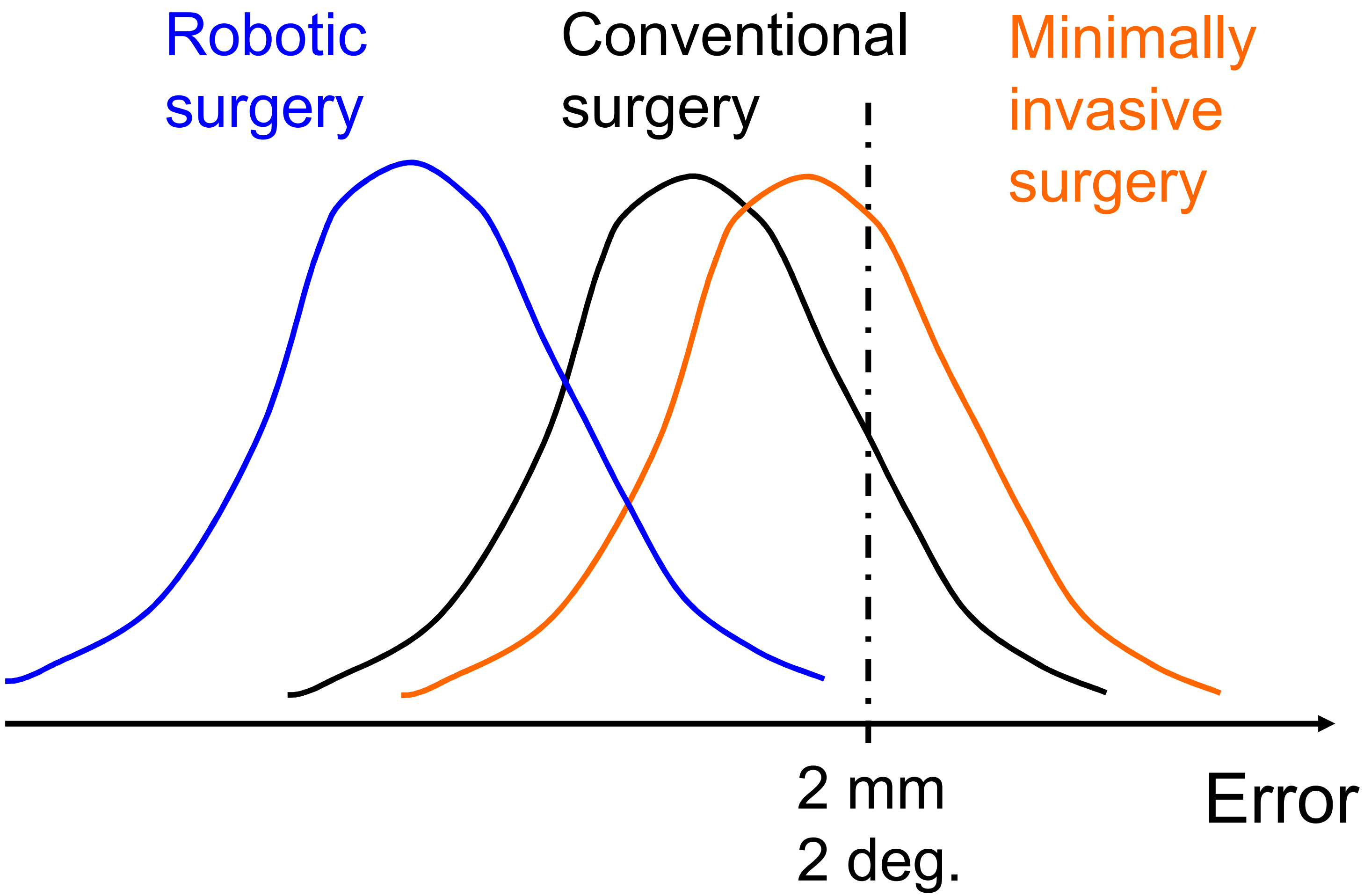

7-axis bone cutting robot

Mechanism

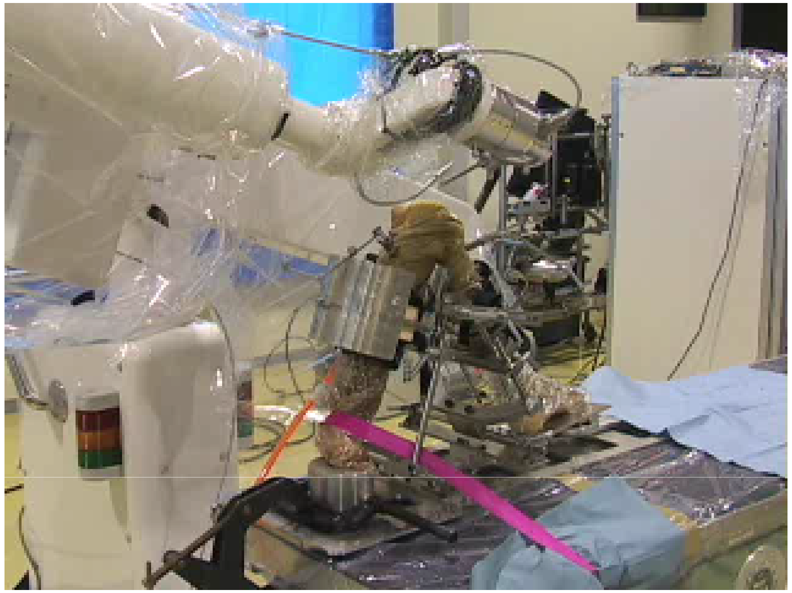

(1) C-arm type structure:
- Adequate workspace,
- A view for a surgeon

(2) 7-axis:
- 3 rotational axes
- 3 precise translational axes
- 1 (Z-axis) coarse translational axis

(3) 2 redundant axes:
- MIS
- Minimizing the total size of the robot

Cutting tool posture control with a redundant axis

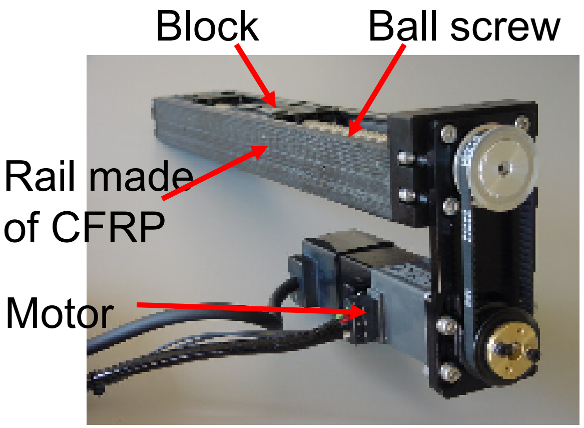

Weight reduction using CFRP

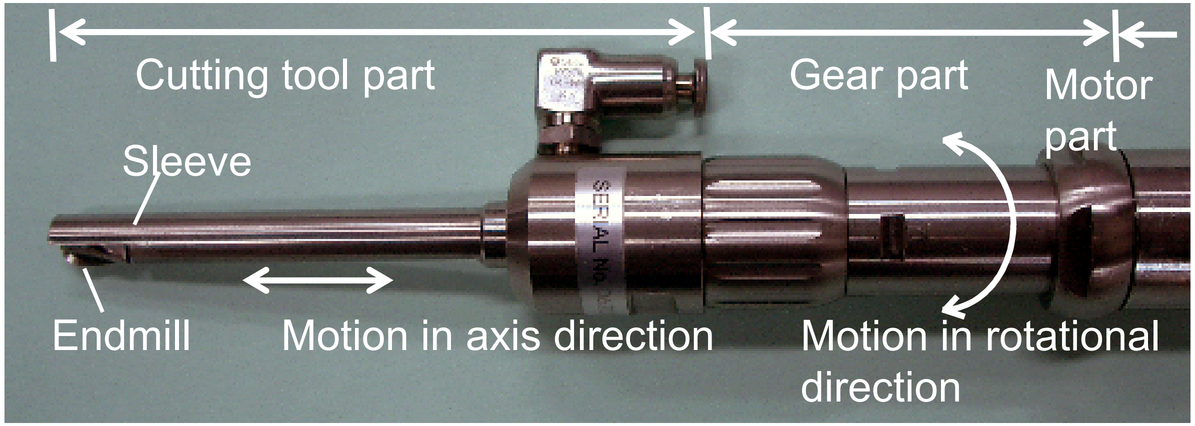

To increase the safety of the system …

Planning for the femur (Determination of the front direction of the femur)

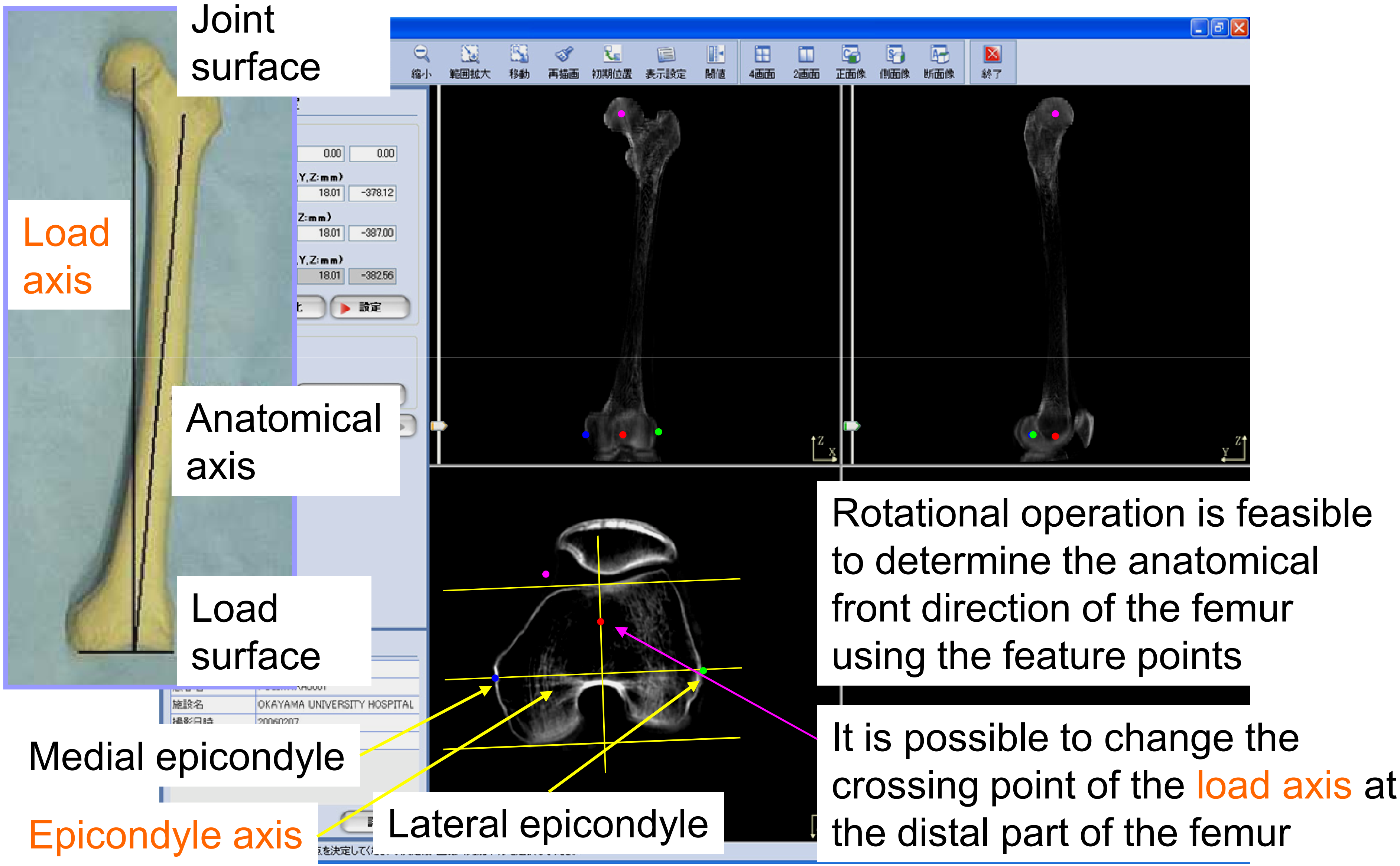

Preoperative CAD system

Confirmation of the alignment for the femur and the tibia

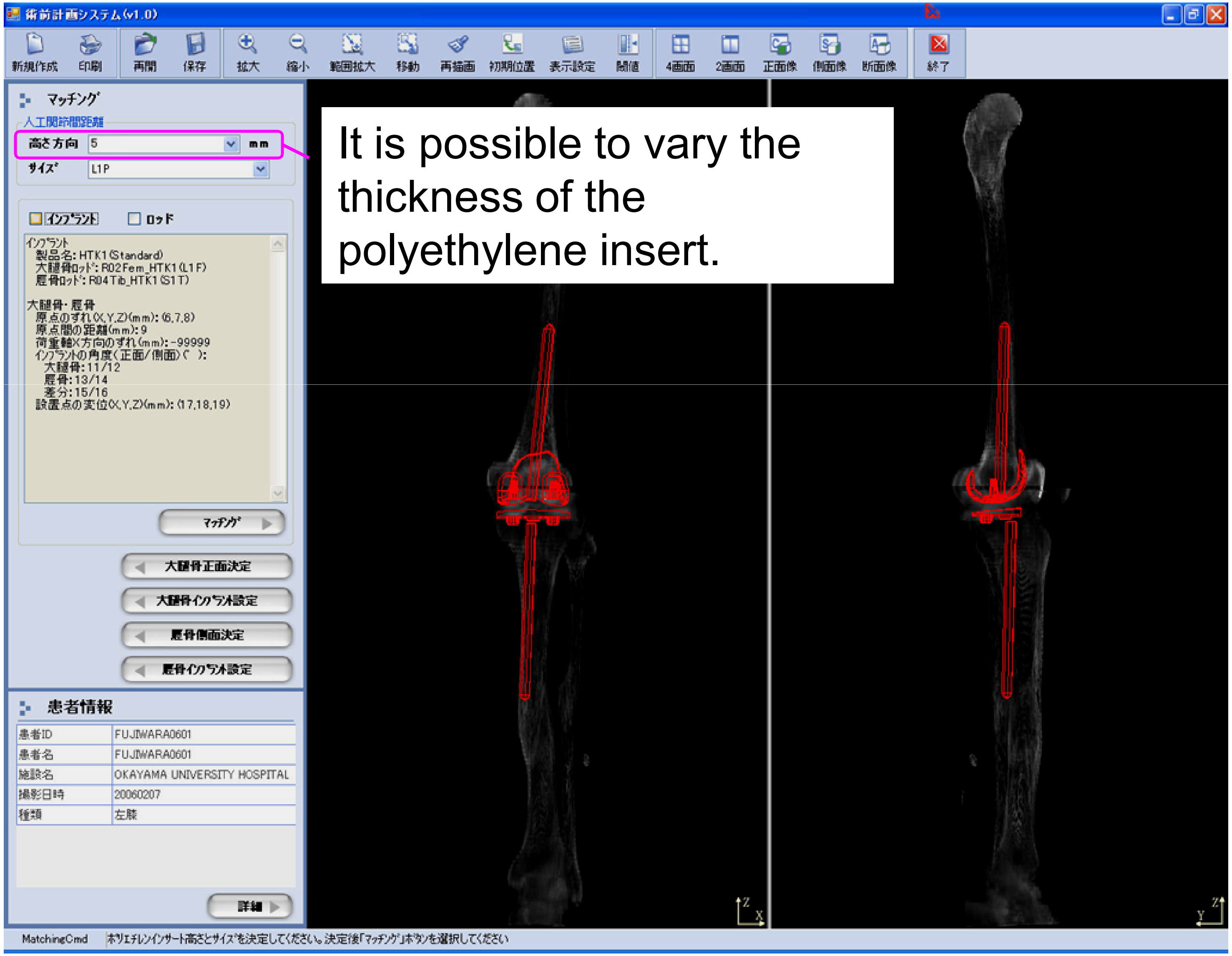

It is possible to vary the thickness of the polyethylene insert.

System construction

Software

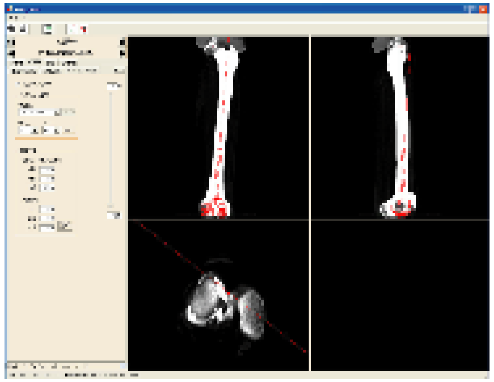

Preoperative planning system (CT-based)

(1) Extraction of bone surface

(2) Characteristic points

(3) Implant size

(4) Implant position

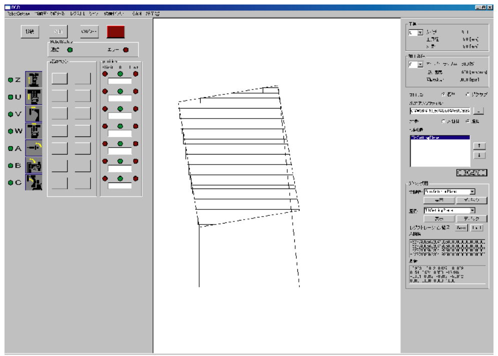

Intraoperative CAM system

(1) Registration

(2) Tool path generation

(3) NC program generation

Hardware

System in an operation room

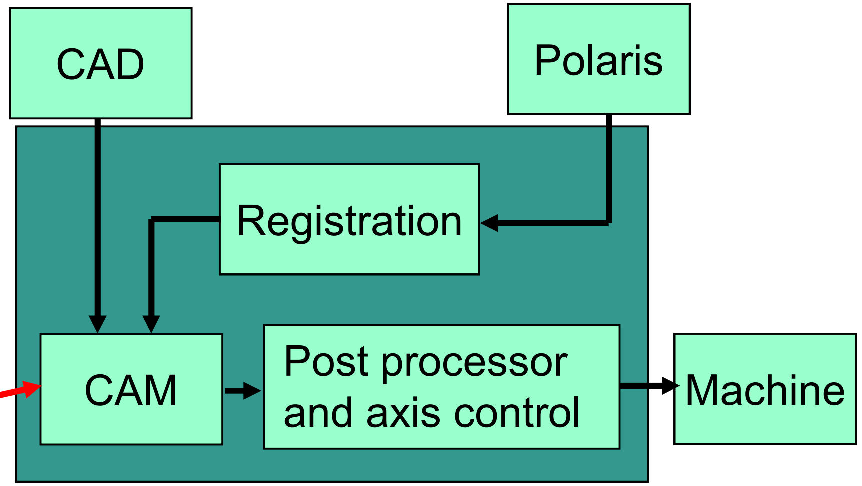

System configuration

Registration

- Infrared coordinate measurement system was adopted to measure the position and the posture of the bone.
- Matching of preplanned and measured points during the surgery

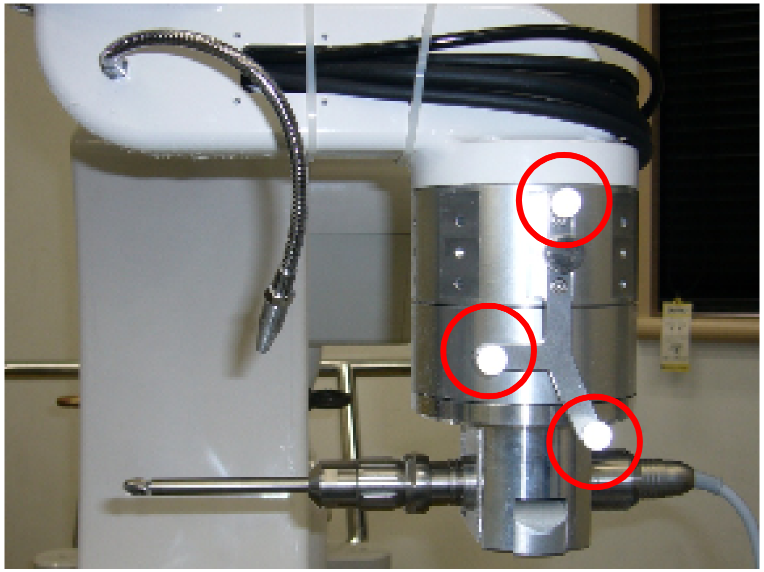

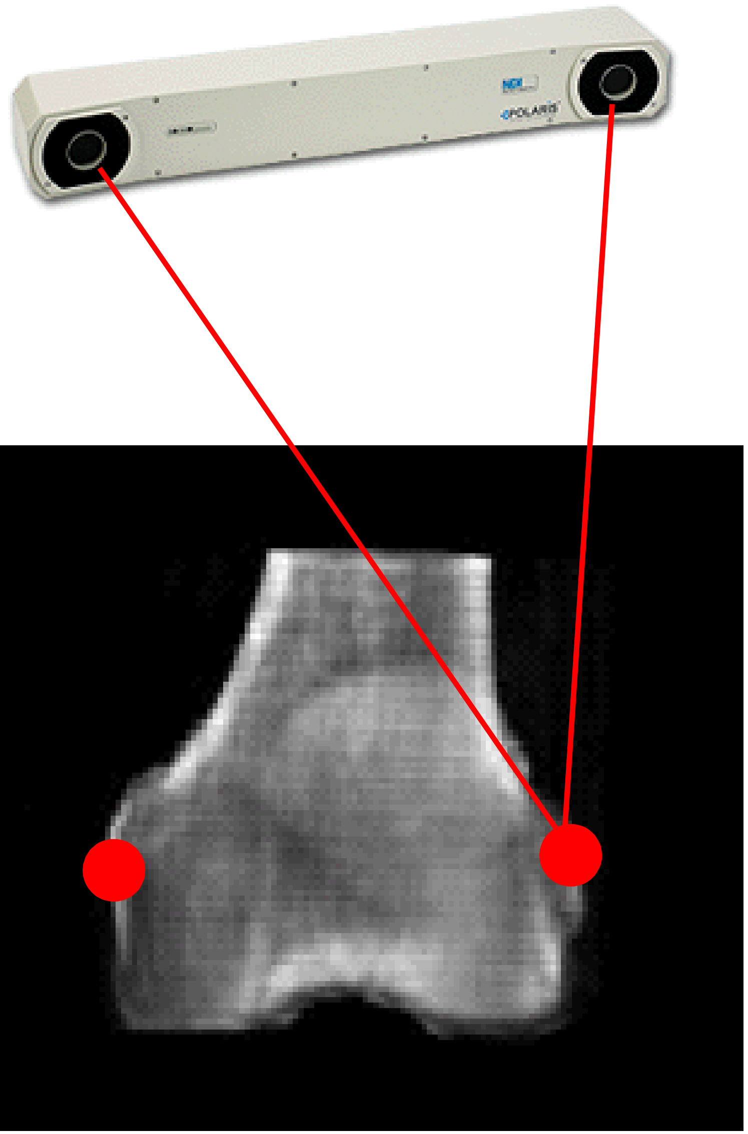

- Position recognition of the bone cutting machine tool

Point matching registration method

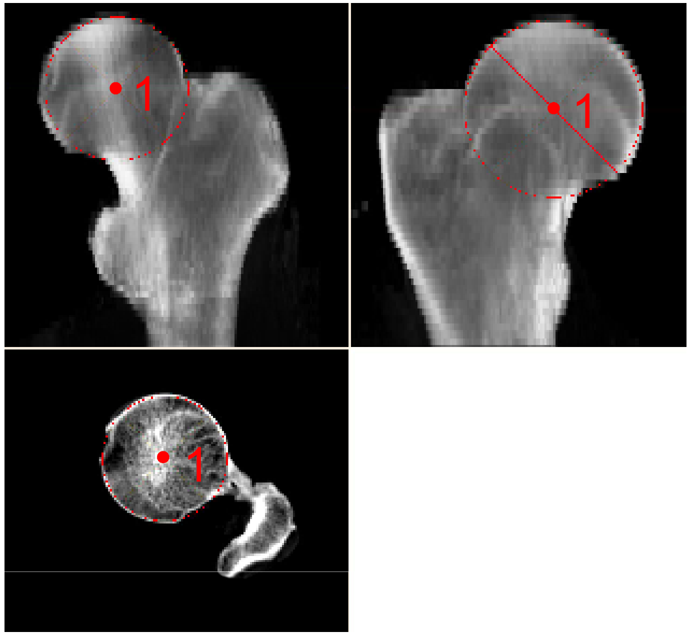

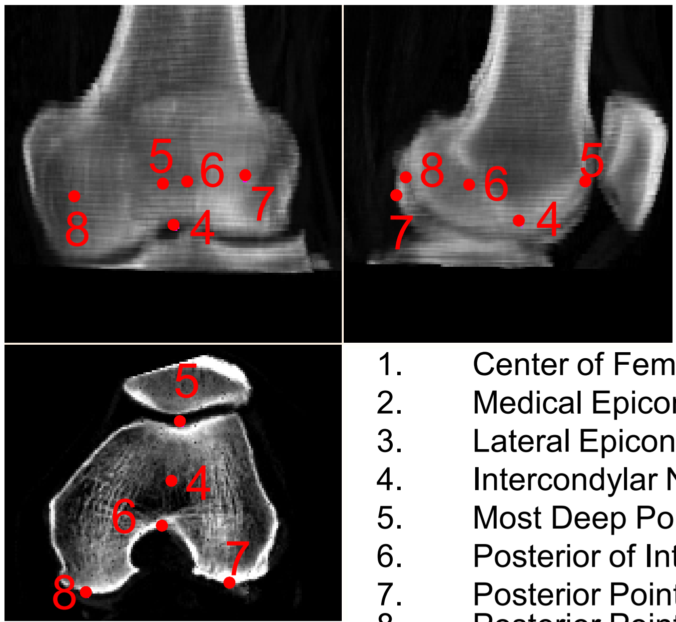

1. Center of Femoral Head
2. Medical Epicondyle
3. Lateral Epicondyle
4. Intercondylar Notch
5. Most Deep Point of Groove
6. Posterior of Intercondylar Notch
7. Posterior Point of Lateral Condyle
8. Posterior Point of Medial Condyle

Point matching registration

Analysis result for “medial epicondyle”:

- Standard deviation (6.10 0.77 0.24)
- Distributed in a line
- Distributed in front and back direction
- No distribution in distal and proximal direction

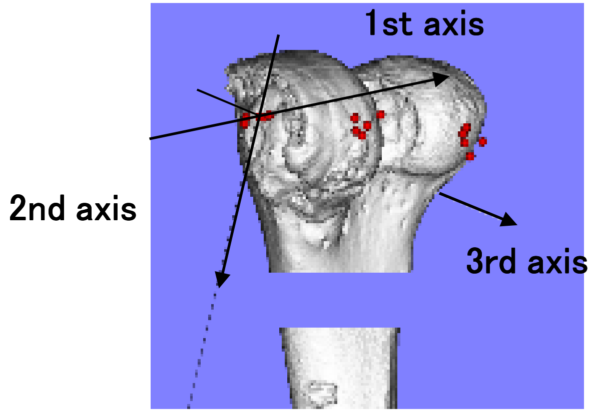

MED

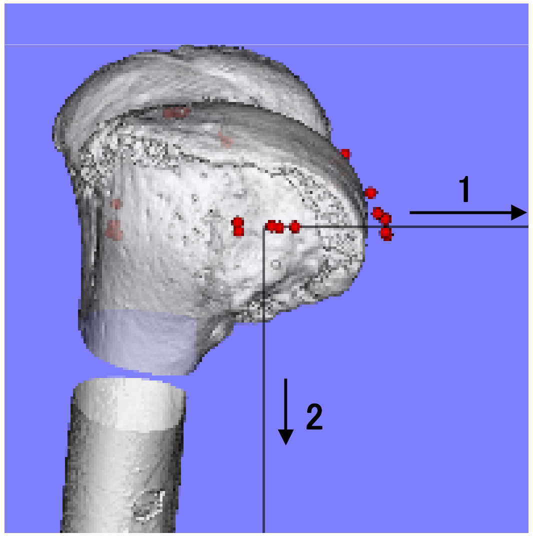

1–2 plane

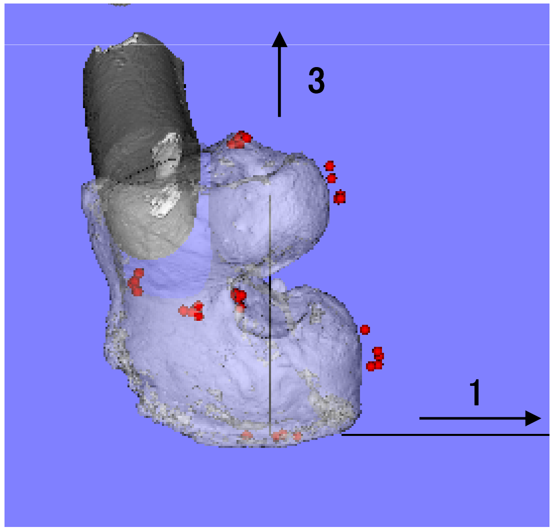

1–3 plane

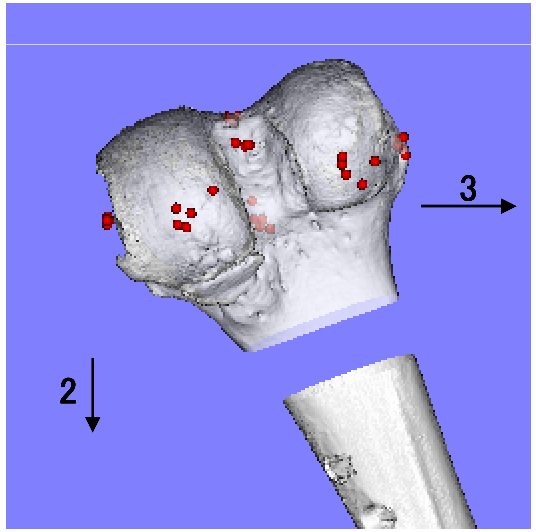

3–2 plane

The accuracy of point matching: ~ 1.5 mm, ~ 1.5 deg.

Registration using the surface information

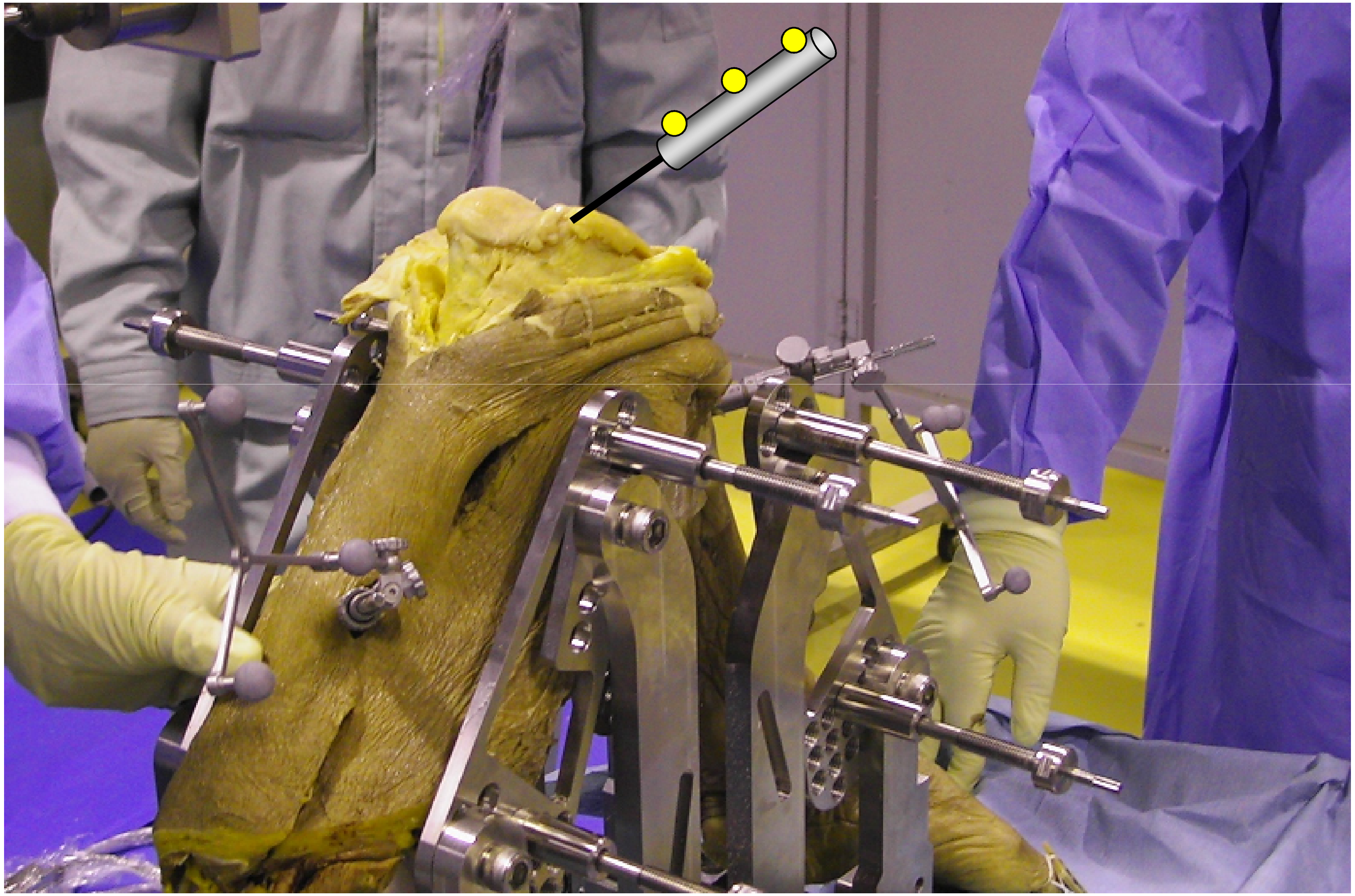

Femur (Front view)

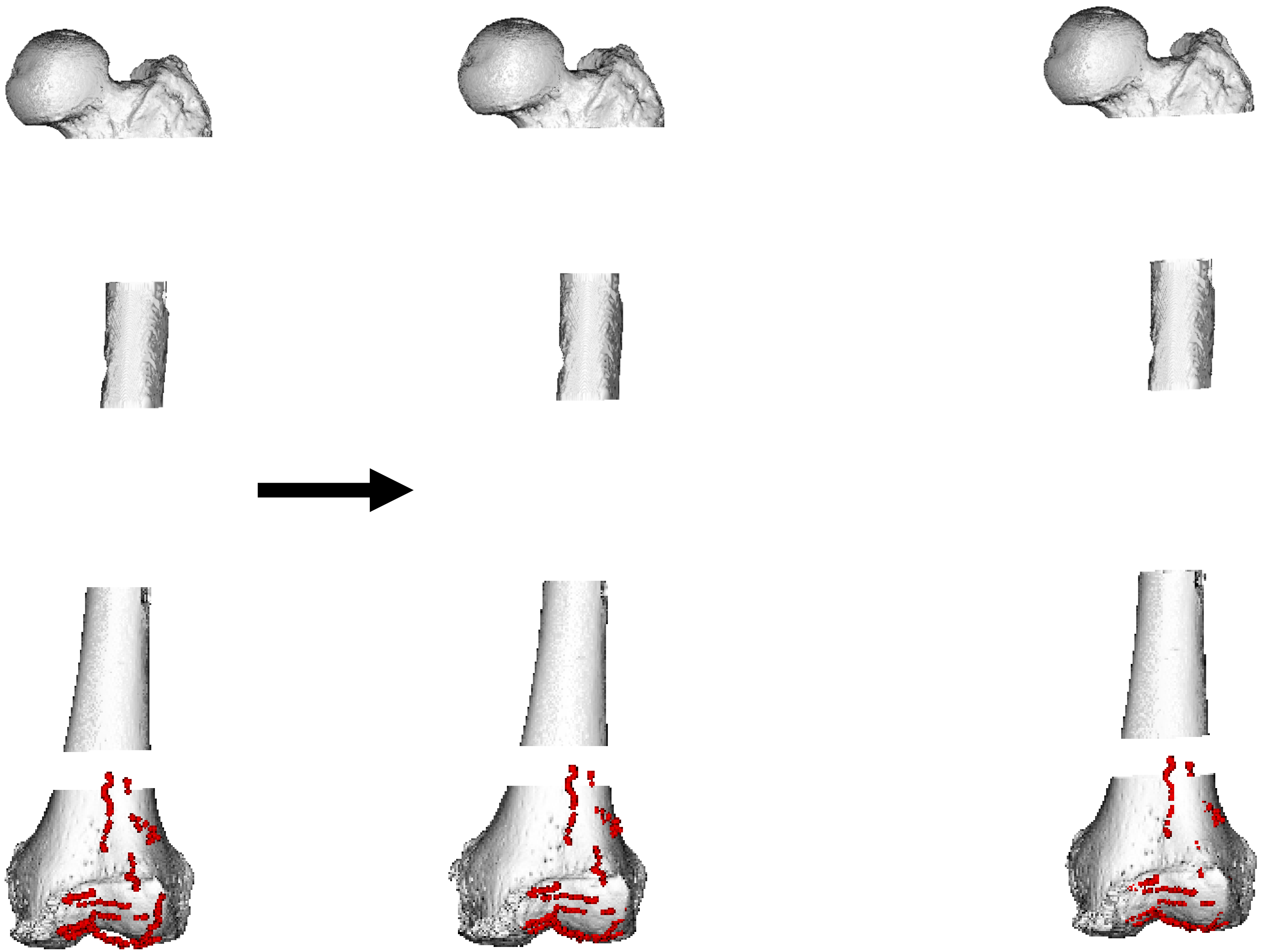

Surface registration

Point matching registration

Femur (Side view)

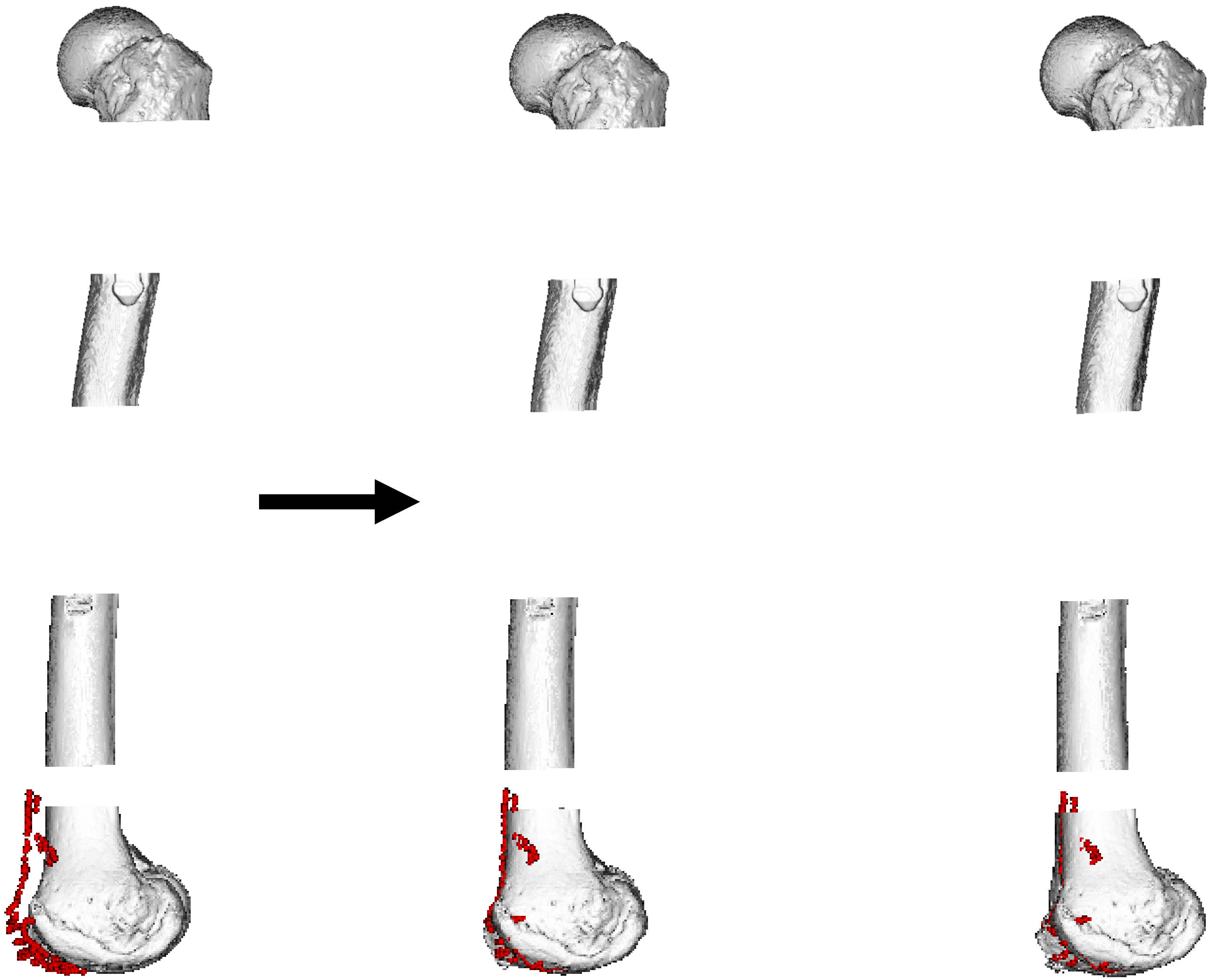

Surface registration

Point matching registration

Surface registration (femur)

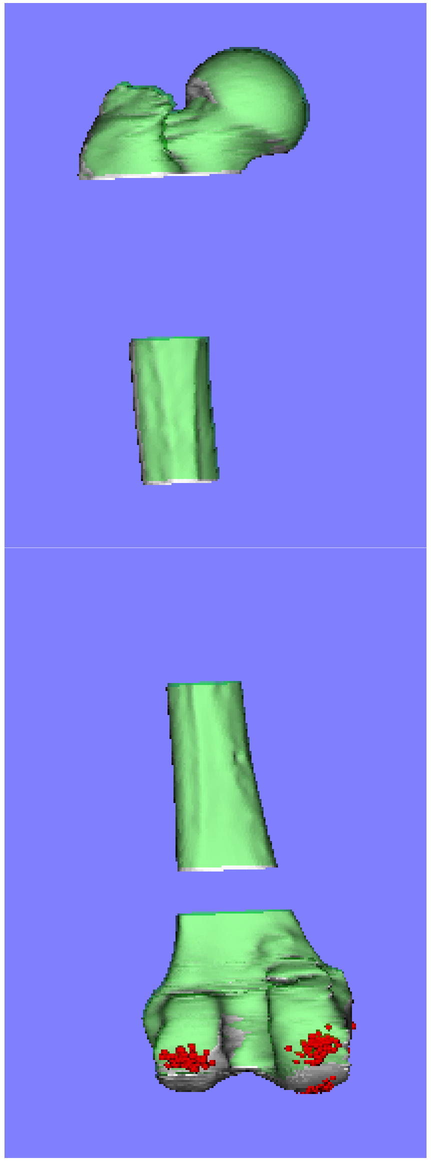

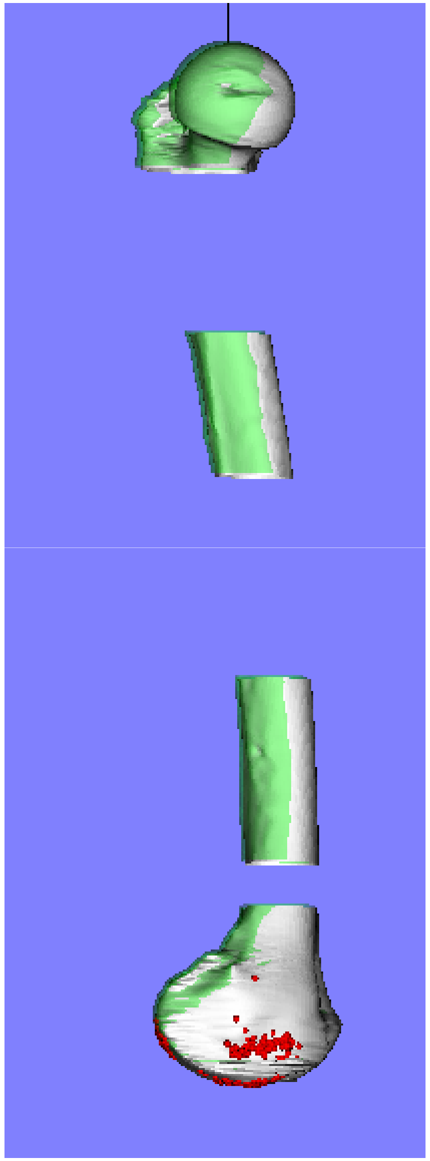

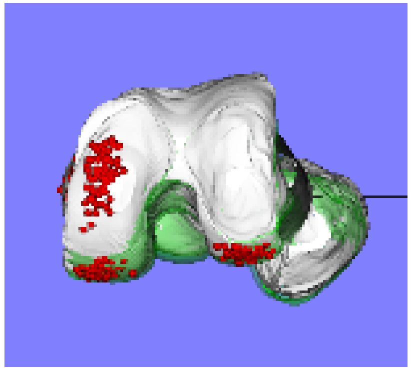

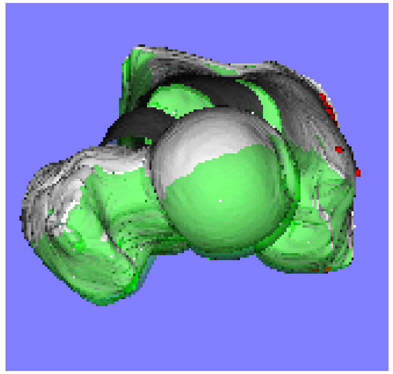

Experimental result:

White: (Available surface area) + (Femoral head) : Residual: 0.52 mm

Green: All surface information (correct answer): Residual: 0.91 mm

Femoral head distance between two models: 3.0 mm

Angle error:

- Front and back direction: 0.22 deg.
- Left and right direction: 0.30 deg.
- Around load axis: 0.17 deg.

Toolpath generation (1)

Modeling of knee joint

(1) Measurement of opening area

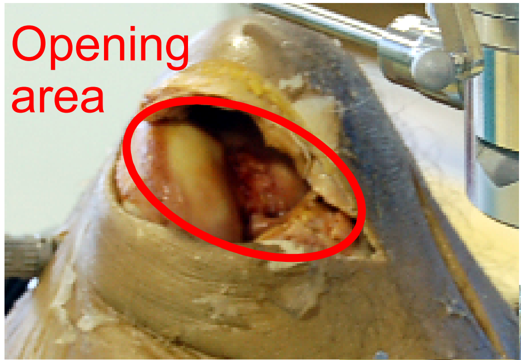

Probe with markers

With a 3-dimensional optical position sensor

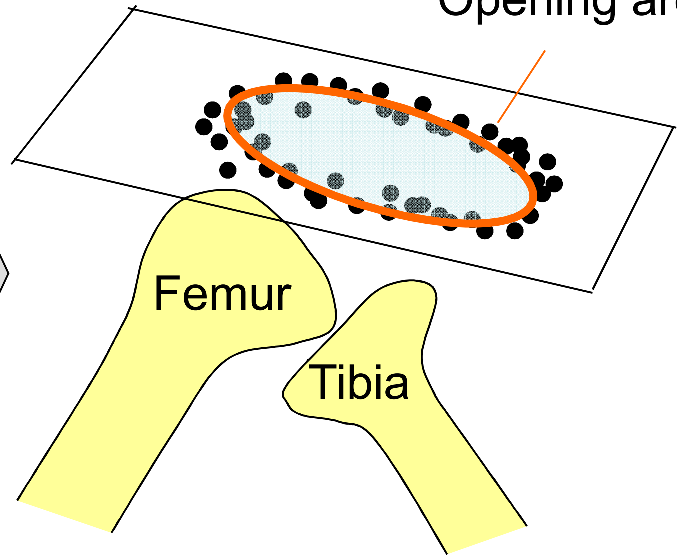

The border of the area is measured as the points for the opening plane.

Regression analysis is used for measured data $\vec{p}_i\,(\,i=1,\ldots)$,

$$J(a,b,c)=\sum(z_i-ax_i-by_i-c)^2$$

$$\frac{\partial J}{\partial a}=0,\frac{\partial J}{\partial b}=0,\frac{\partial J}{\partial c}=0$$

is calculated

A plane $z=ax+by+c$ is obtained.

(2) Measurement of obstacles

Area which cutting tool should not contact (soft tissue, nerves, vessels, etc.) is measured and calculated.

Toolpath generation (2)

Setting plane of UKA

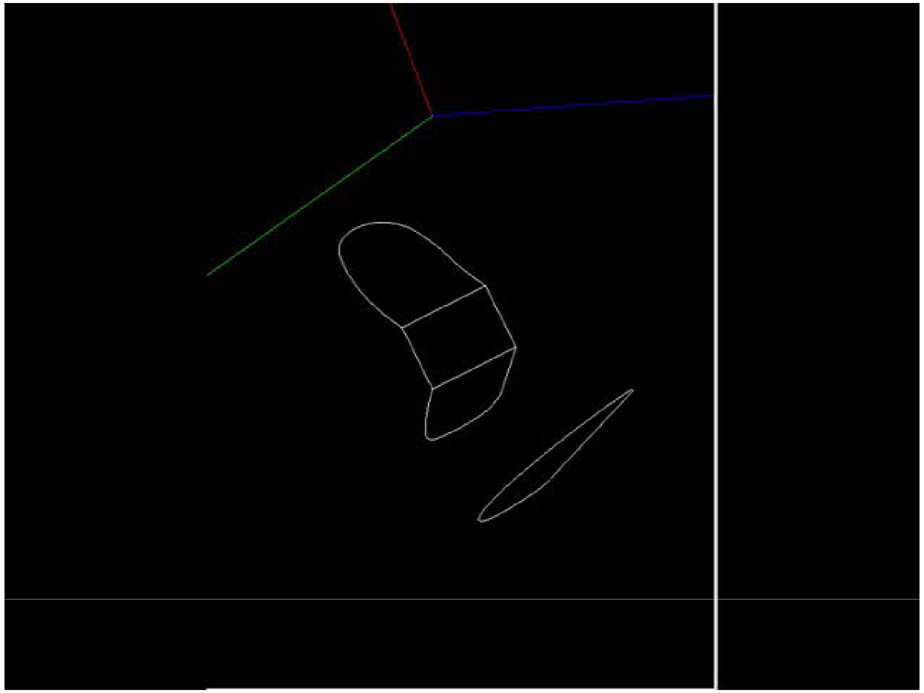

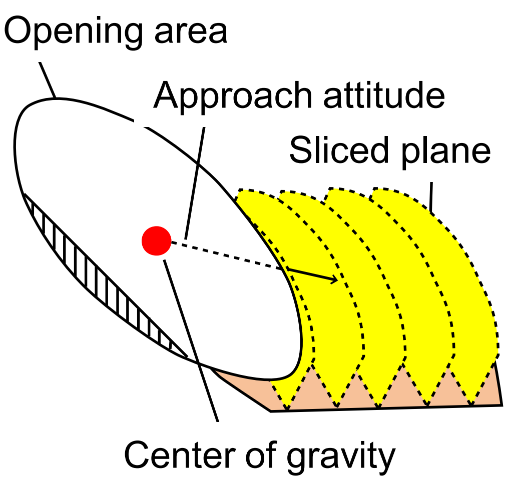

(a) Generation of cutting planes

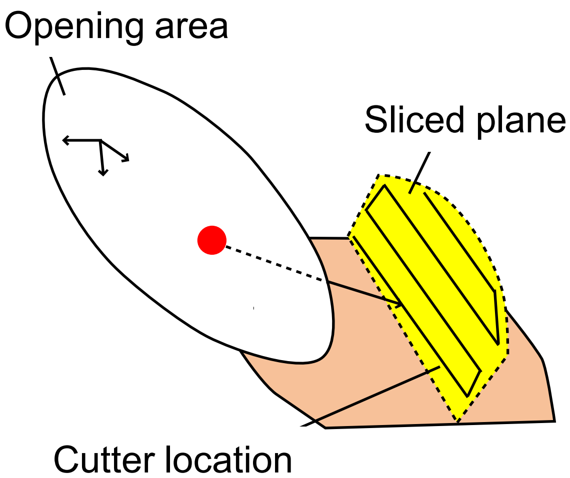

(b) Generation of cutter location

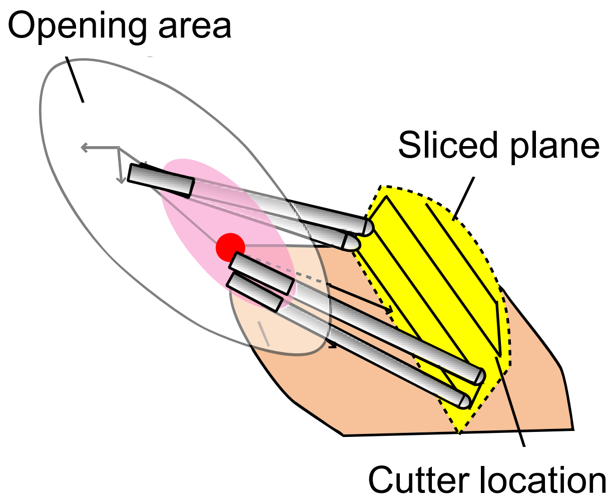

(c) Calculation of tool posture

Control algorism

- Control around the tool rotation axis

  Part which is not contributing for cutting should be covered.

- Control along the tool rotation axis

  The covering amount is determined by the angle between the cutting tool and the resection plane:

  α large -> pull
  α small -> push

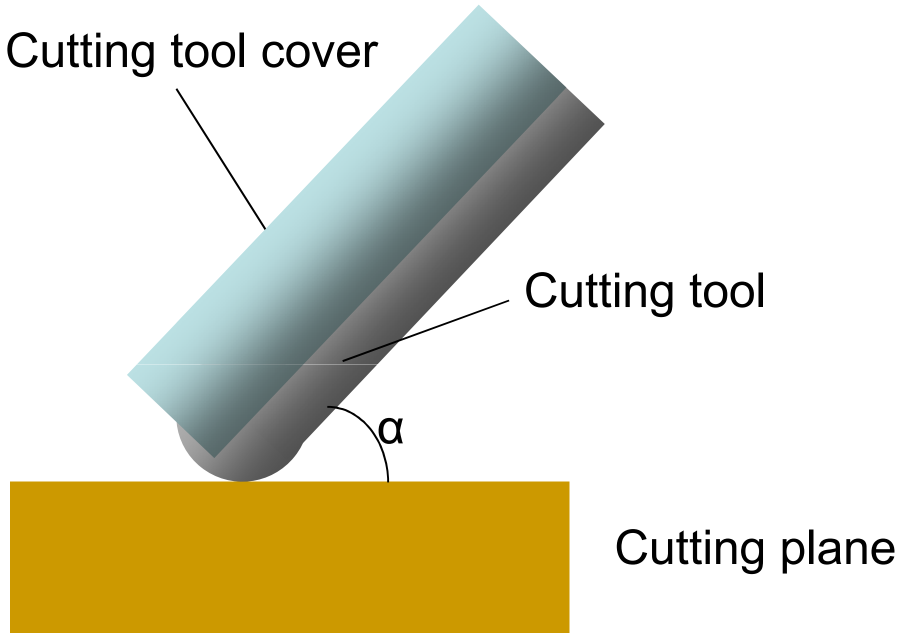

α: Angle between cutting tool and plane

Angle control of cutting tool cover

Direction vector $\underline{a}$ is defined when the rotational angle is 0 degree and the cutting tool is located at the home position.

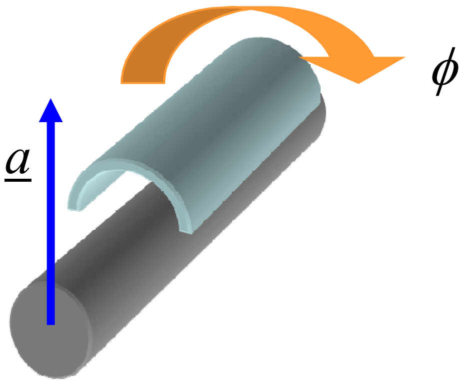

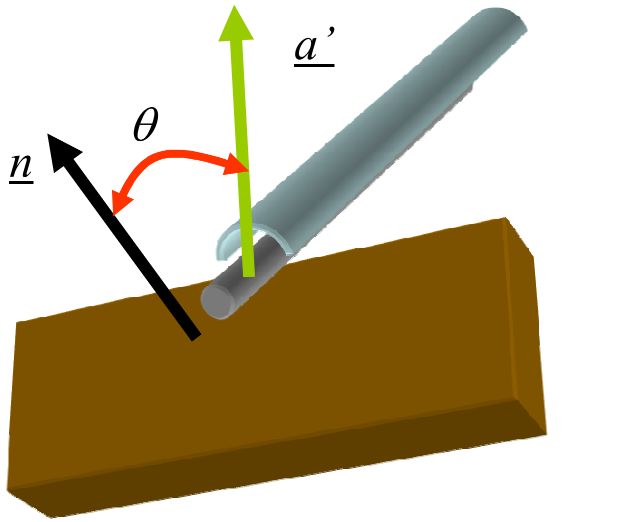

Attitude of the robot — Angle of the cutting tool cover

$$\underline{a}' = E^B \cdot E^C \cdot E^A \cdot E^\phi \underline{a}$$

$$\underline{a}' \cdot \underline{n} = |\underline{a}'||\underline{n}'| \cos\theta = f(\phi)$$

$\underline{n}$: Normal vector of the cutting plane

ϕ is controlled to minimize θ .

ϕ is determined to maximize $\underline{a} \cdot \underline{n}$.

Bone cutting experiment using a cadaver

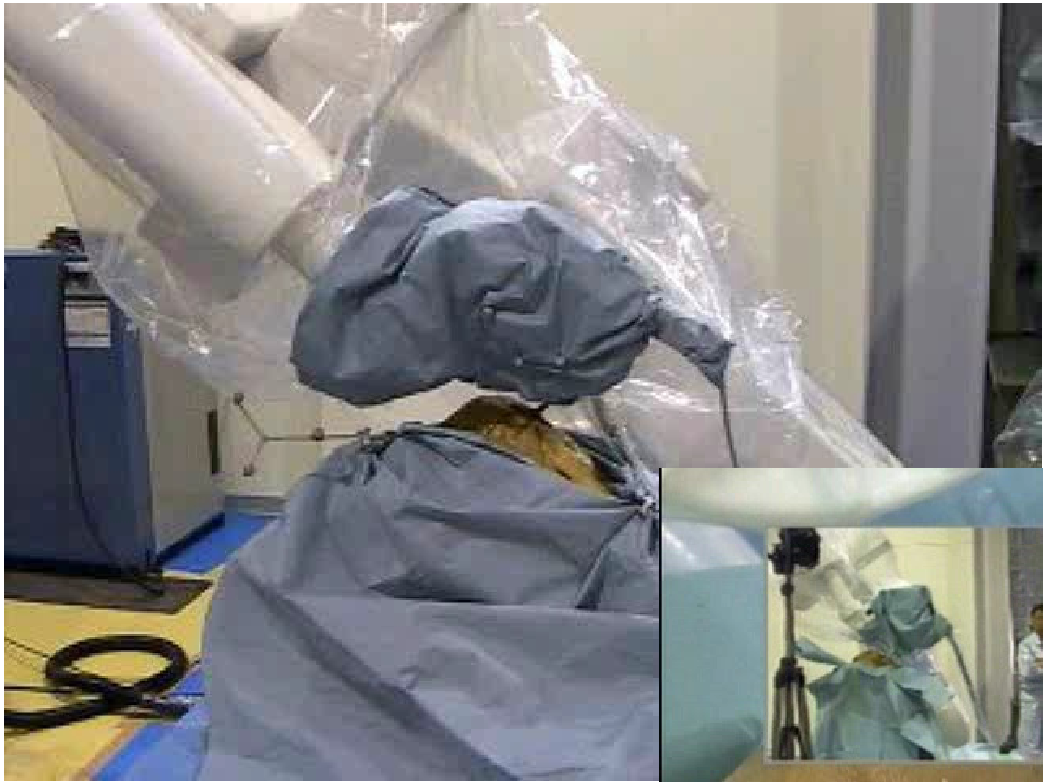

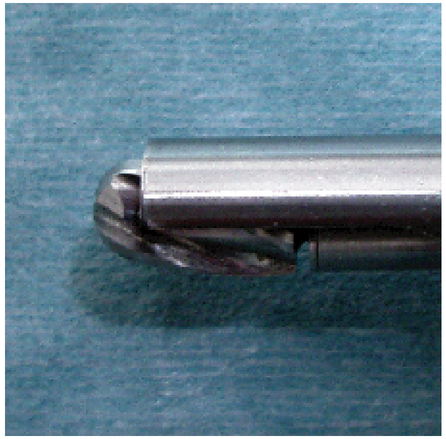

3D measurement

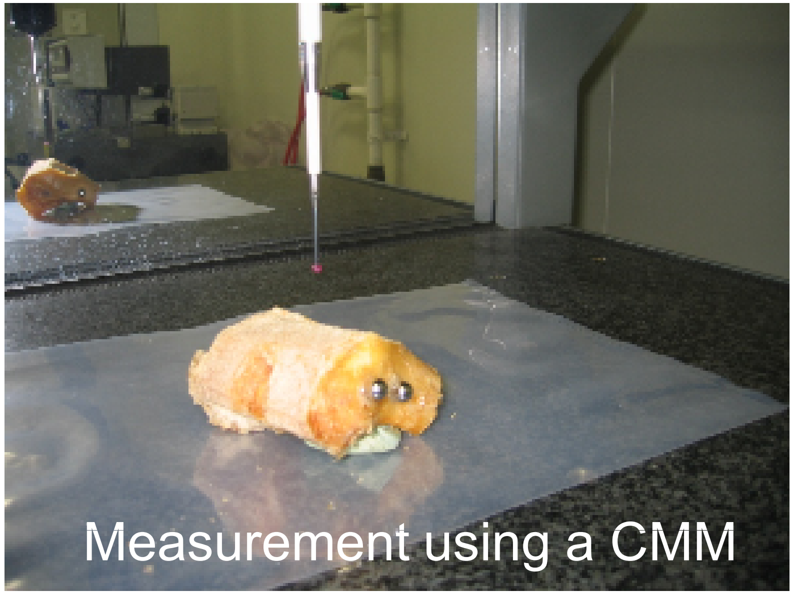

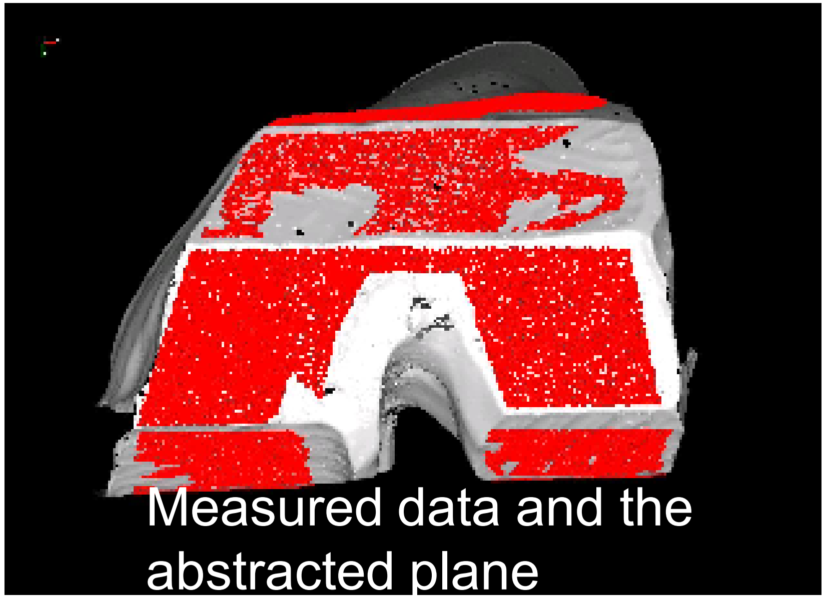

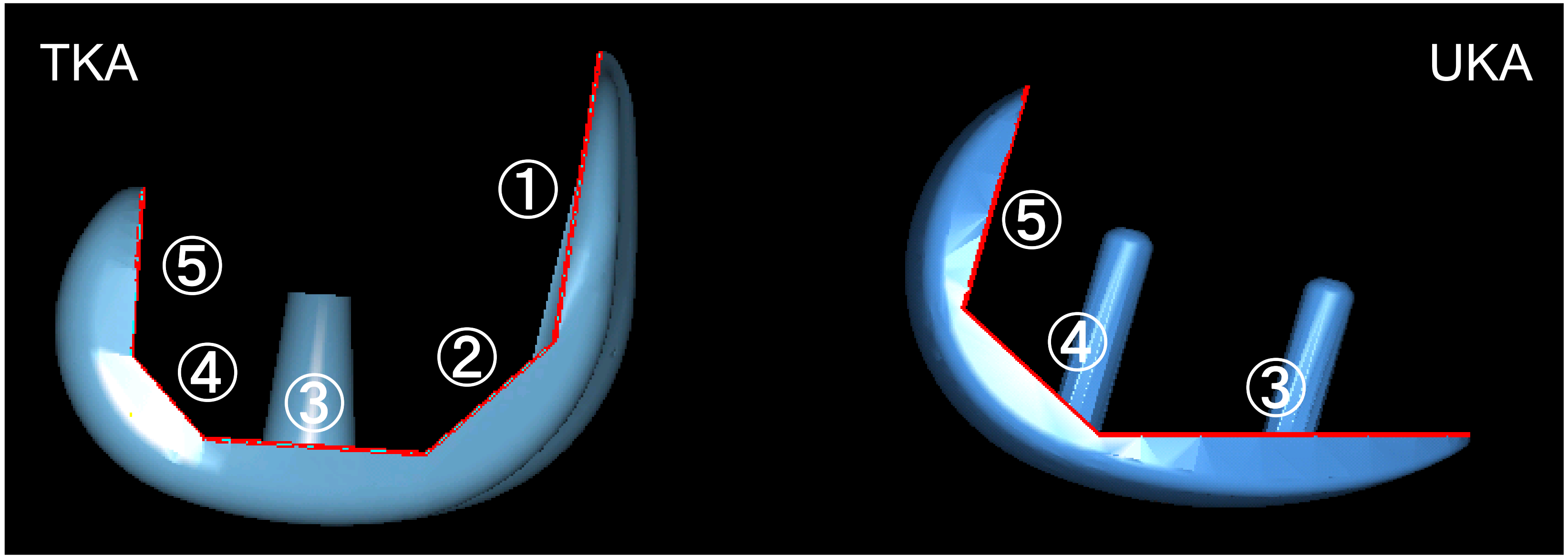

Shape accuracy of the cutting plane

Plane	3786L (TKA)			3833L(UKA)			3833R (UKA)			Ave. error
	Plan	Meas.	Err.	Plan	Meas.	Err.	Plan	Meas.	Err.	
1−2	140.0	140.1	0.1							0.1
1−3	85.0	84.1	0.9							0.9
1−4	50.0	49.5	0.5							0.5
1−5	5.0	6.1	1.1							1.1
2−3	45.0	44.2	0.8							0.8
2−4	90.0	89.3	0.7							0.7
2−5	135.0	134.0	1.0							1.0
3−4	135.0	133.6	1.4	135.0	135.8	0.8	135.0	134.7	0.3	→ 0.8
3−5	90.0	89.8	0.2	75.0	75.8	0.8	75.0	75.8	0.8	→ 0.6
4−5	135.0	136.6	↓ 1.6	120.0	119.9	↓ 0.1	120.0	121.1	↓ 1.1	→ ↓ 0.9
Ave. err			0.8			0.6			0.7	→ 0.7

Evaluation of alignment and position accuracy

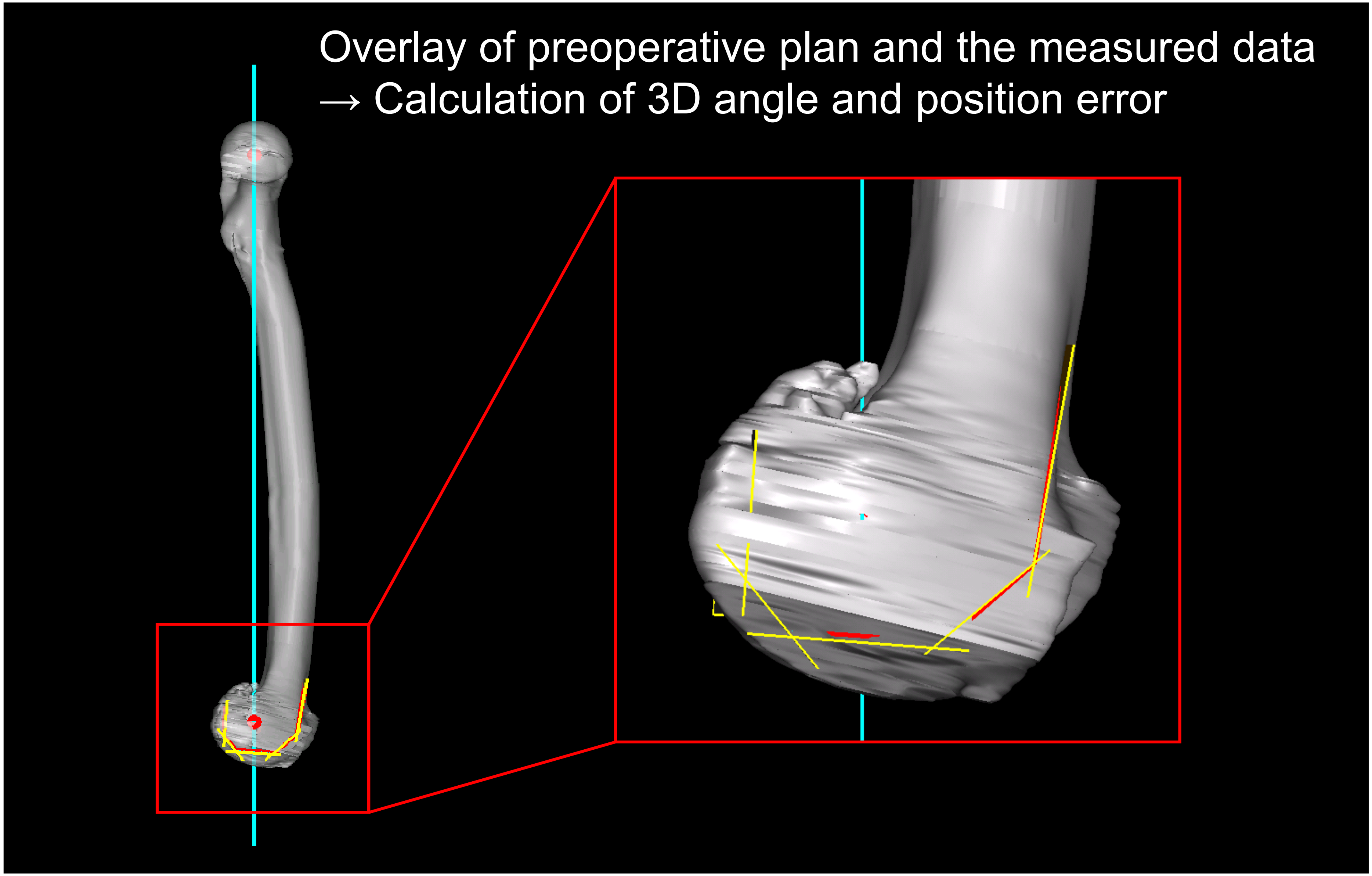

Evaluation axis

Femur: Load axis – Distal plane (TKA: 86 deg., UKA: 90 deg.)

Tibia: Load axis – Proximal plane (90 deg.)

Femur: SEA – Posterior plane (0 deg.)

Tibia: -

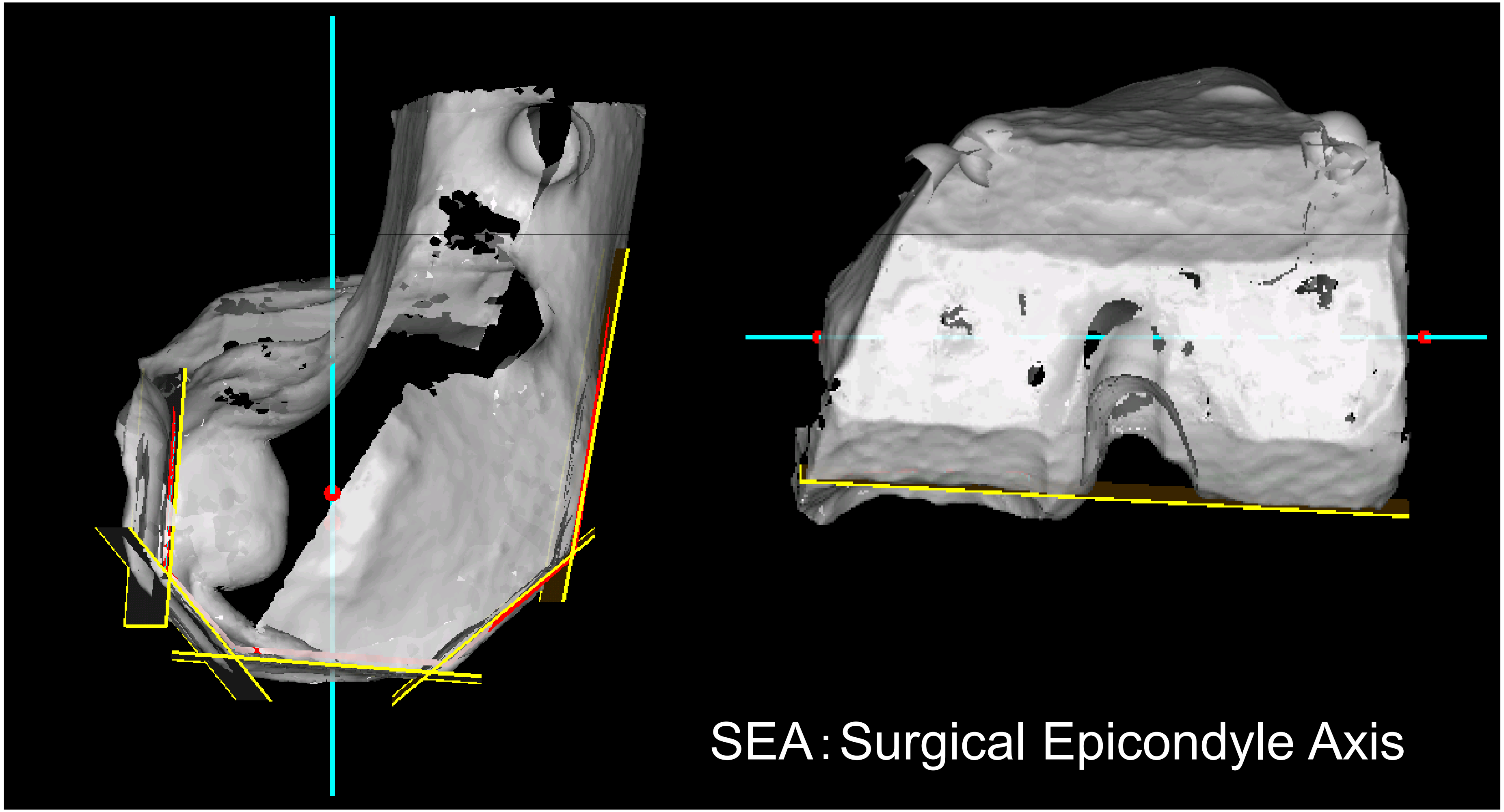

Alignment and position accuracy

(Planed) – (Measured)	Position error [mm]			
	3786L	3833L	3833R	Ave. error
Plane3 (Distal)	1.21	1.18	1.01	1.13
Plane5 (Posterior)	0.42	0.97	1.23	0.87
Tibia	0.60	0.27	0.61	0.49
Average error	0.74	0.81	0.95	0.83

Position precision: 1.0 mm

(Plane) - (Axis)	Angle error [deg]			
	3786L	3833L	3833R	Ave. error
(Plane3) - (Load axis)	0.6	1.0	0.9	0.7
(Plane5) - (SEA)	3.3	0.5	0.8	1.7
(Tibia) - (Load axis)	1.0	0.2	0.3	0.5
Average error	1.6	0.6	0.7	1.0

Alignment: 1.0 deg.

Temperature measurement: Up cutting / down cutting - Experiment -

Result:

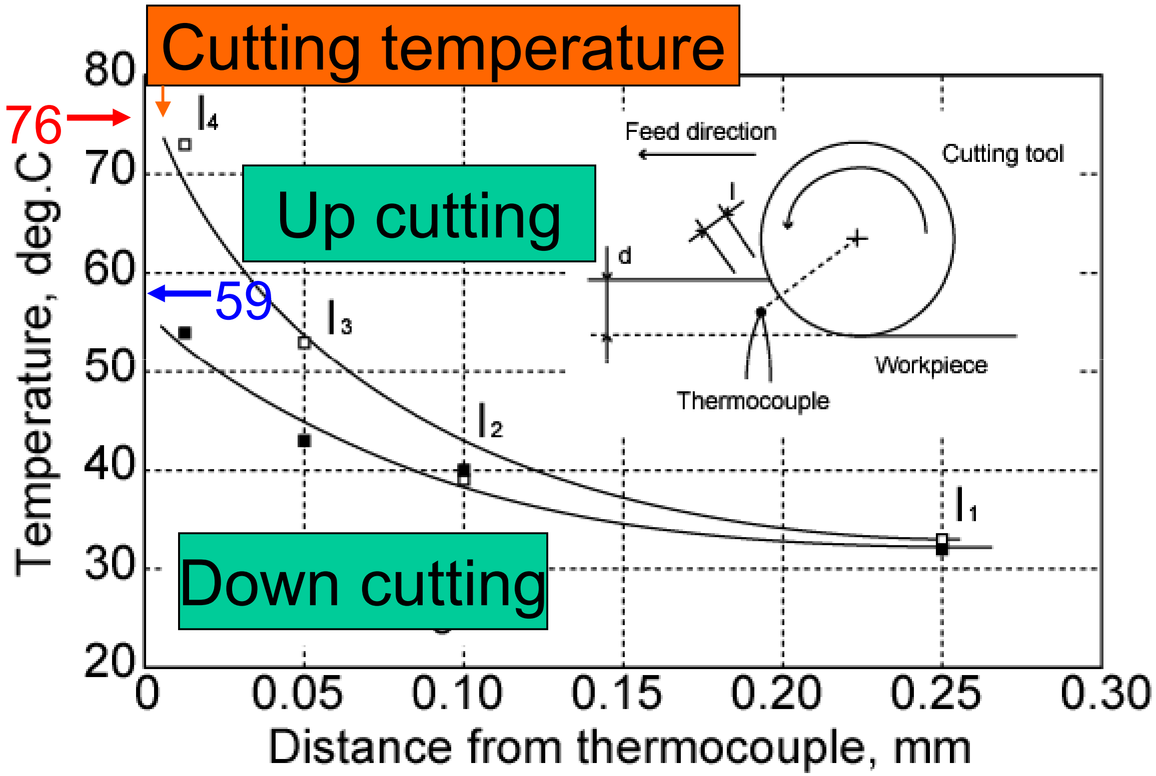

< Condition >

Cutting speed: 31.4m/min, Feed per tooth: 0.375mm/t

Cutting tool diameter: 10mm, 2 flutes square endmill

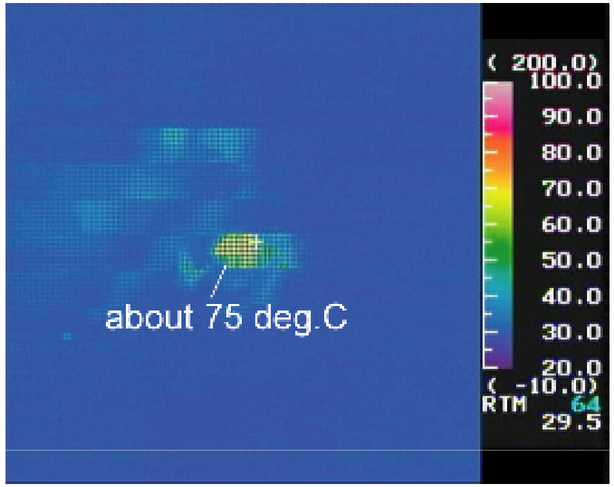

(a) Up cutting

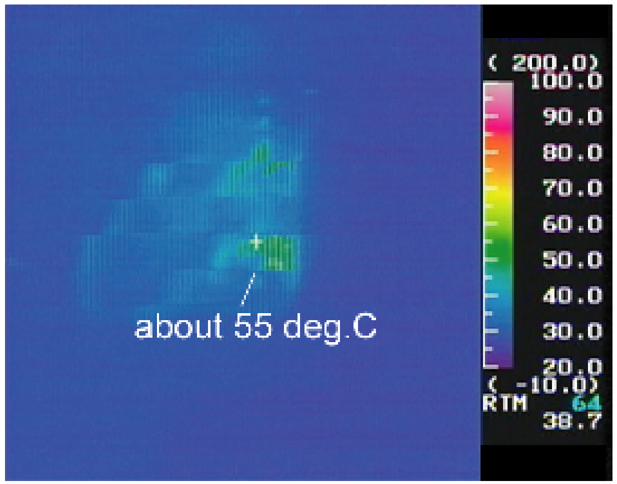

(b) Down cutting

Bone structure

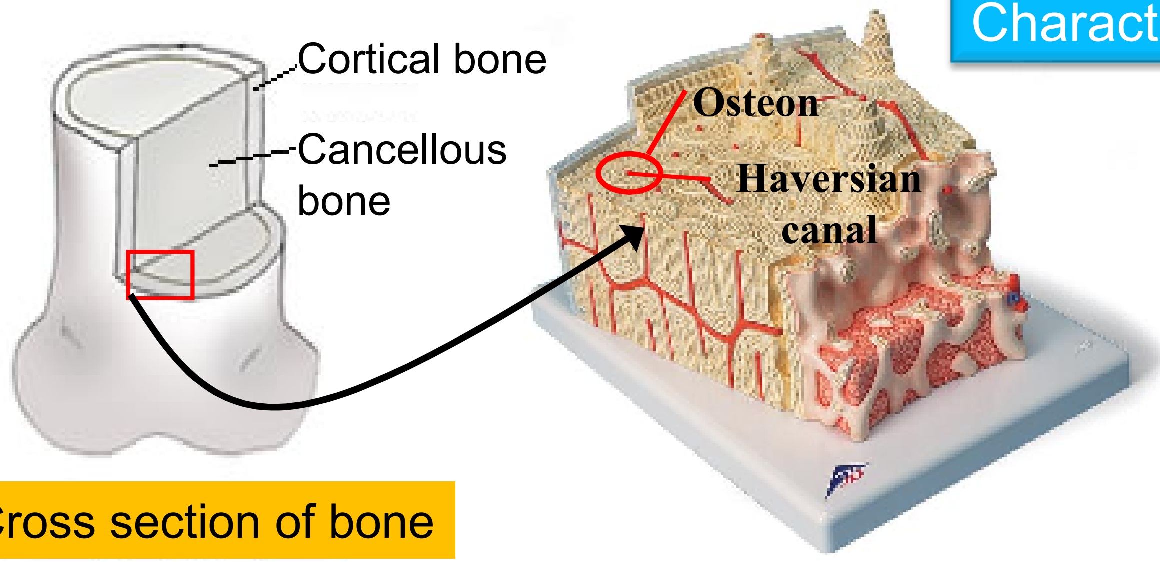

Cross section of bone

Anisotropic

Characteristics of the cortical bone

Across:
Shear stress is small.

Parallel:
Compress stress is large.
Tensile stress is small.

Transverse:
Shear stress is large.

Cutting of cortical bone

3 directions are mixed around the joint part.

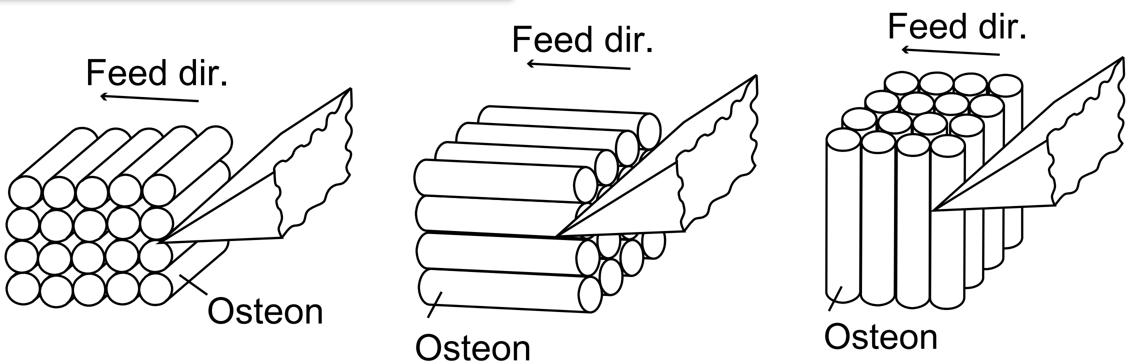

Across   Parallel   Transverse

Cutting characteristics are investigated in 3 directions.

Observation of micro cutting

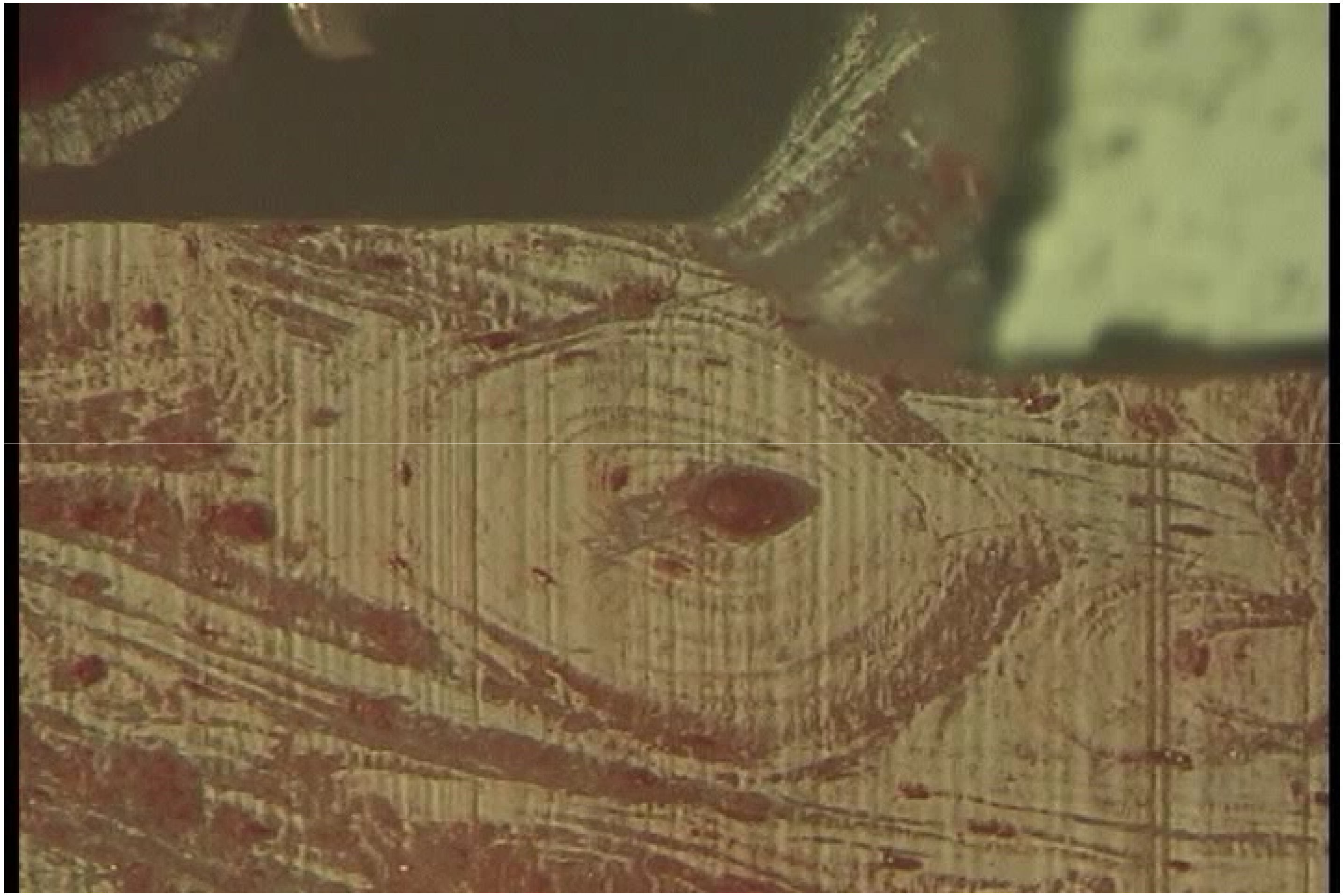

Cow, cortical bone, wet, depth of cut: 80 micrometer

Cutting characteristics of the cortical bone

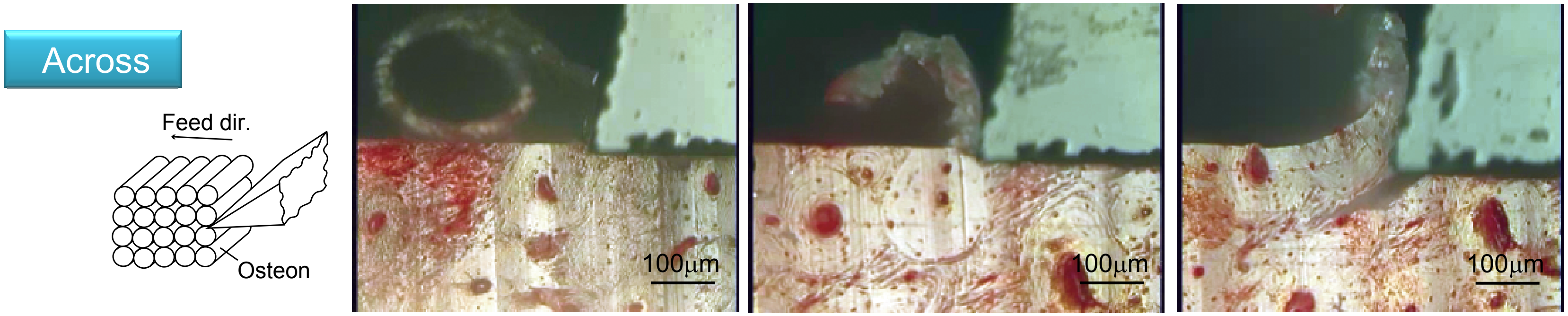

Depth of cut: 10 µm | Depth of cut: 40 µm | Depth of cut: 70 µm

(a) Across

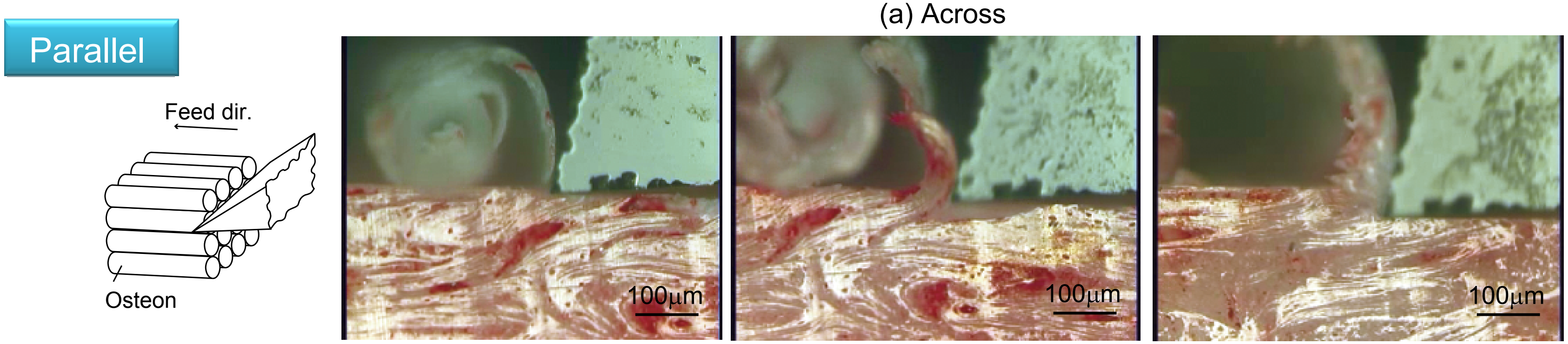

Depth of cut: 10 µm | Depth of cut: 40 µm | Depth of cut: 70 µm

(b) Parallel

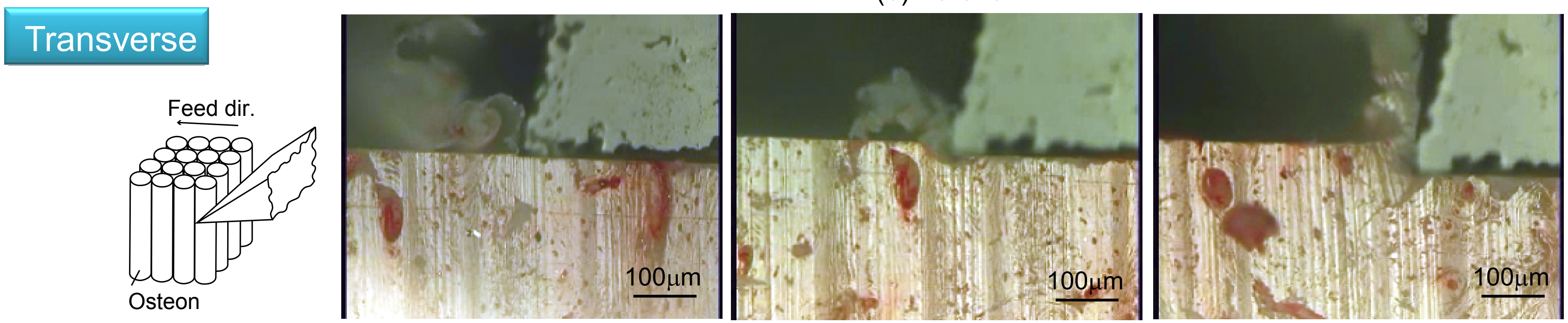

Depth of cut: 10 µm | Depth of cut: 40 µm | Depth of cut: 70 µm

(c) Transverse

Proposed cutting method

(1) High efficiency cutting: Utilization of crack propagation by the impact force.

(2) Low temperature cutting: Actual cutting energy reduction by crack generation.

(3) High precision cutting: Surface roughness is increased by reducing the actual depth of cut.

Cutting cycle

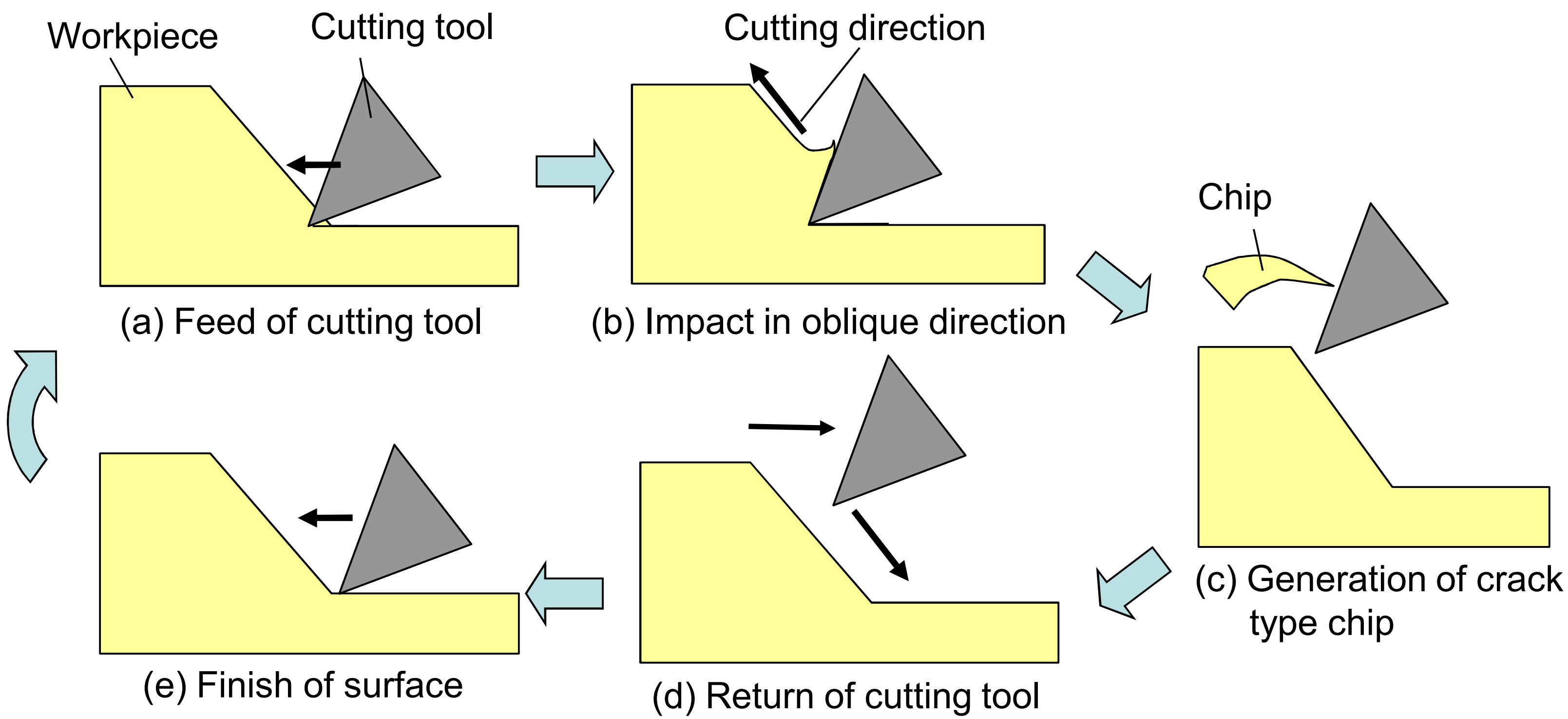

Evaluation experiment while varying the tool feed angle

Experiment condition: cutting depth 100 μm, feed speed 3mm/s, tool rake angle:20 deg.

Cutting resistance

Shear type cutting chips by compress (shear) stress

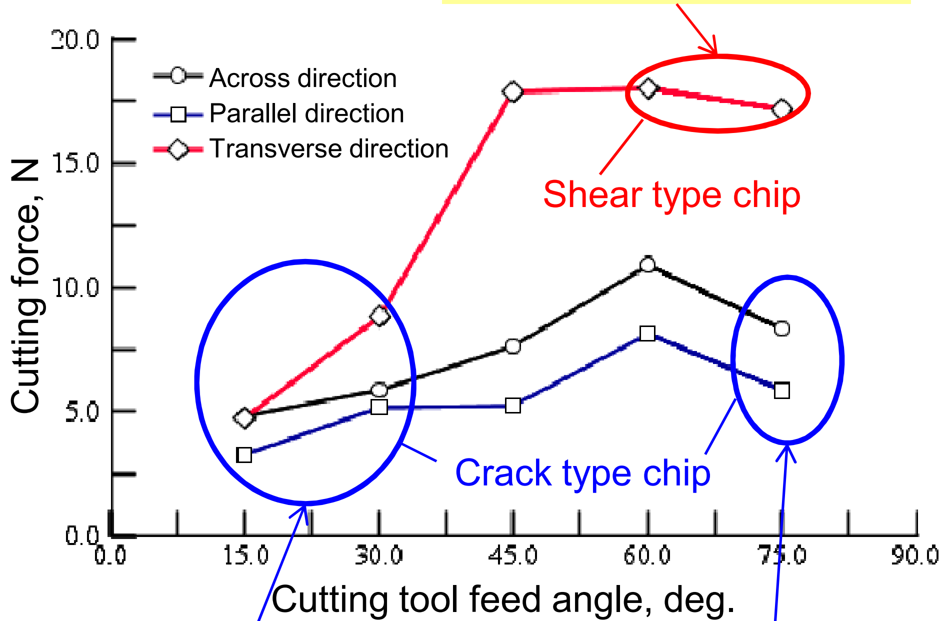

Crack type cutting chips by tensile stress

Crack type cutting chips by compress (shear) stress

- Cutting resistance could be reduced by generating the crack type cutting chips.

Surface roughness

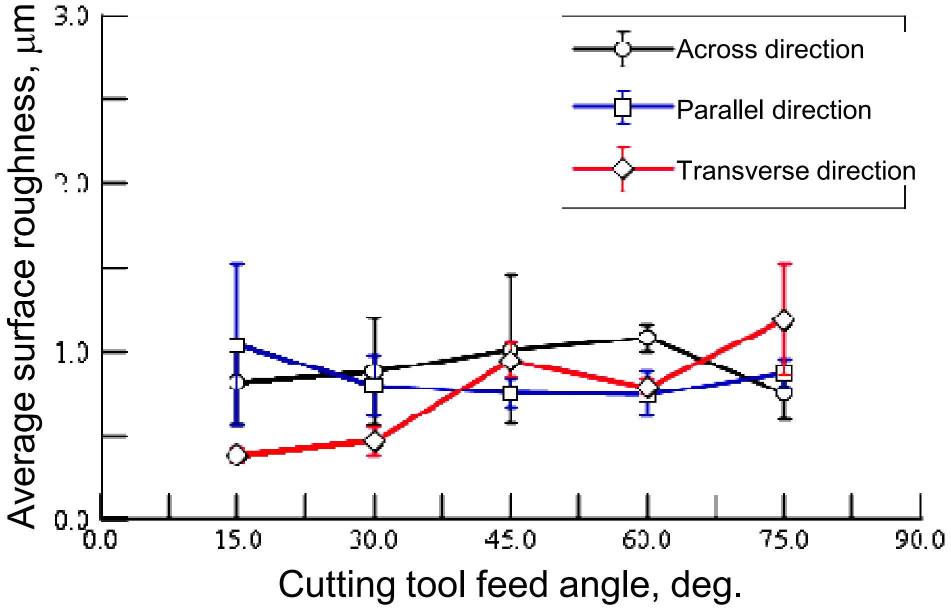

- Good finished surface roughness was obtained independent of the tool feed direction.

Finished surface roughness

Surface roughness

Experiment condition: cutting depth :100 μm,
feed speed: 3 mm/s, tool rake angle: 20 deg.

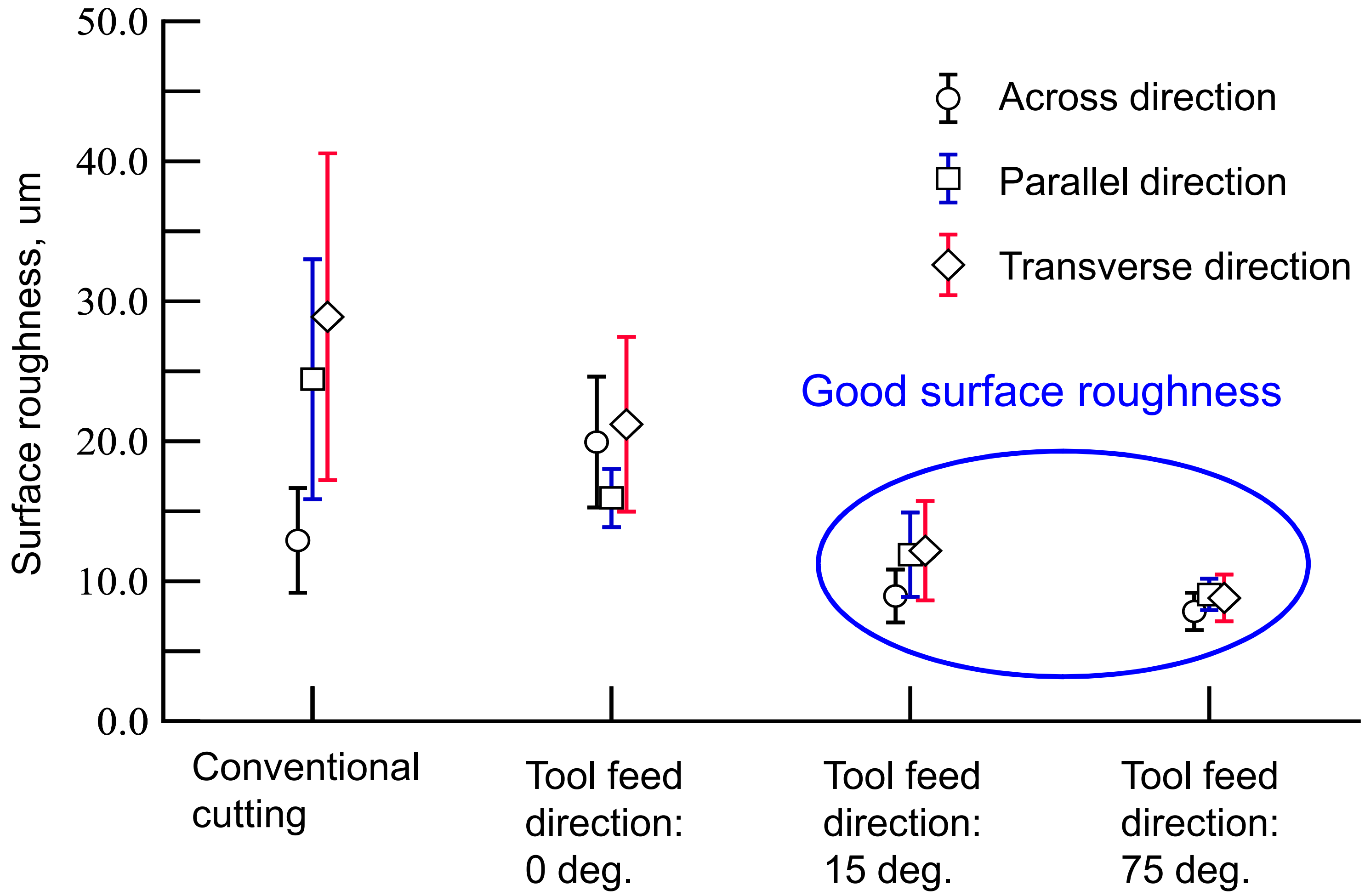

Telesurgery experiment between Japan and Thailand

[Purpose]

– Confirmation of the telesurgery capability using the conventional network

– Confirmation of the effectiveness of the low latency CODEC

[Method]

– A cholecystechtomy and a Nissen fundoplication were performed between Japan and Thailand (distance: 3,750 km) by connecting JGN2 on a pig (female, 3-month old, 30 kg).

Slave manipulator

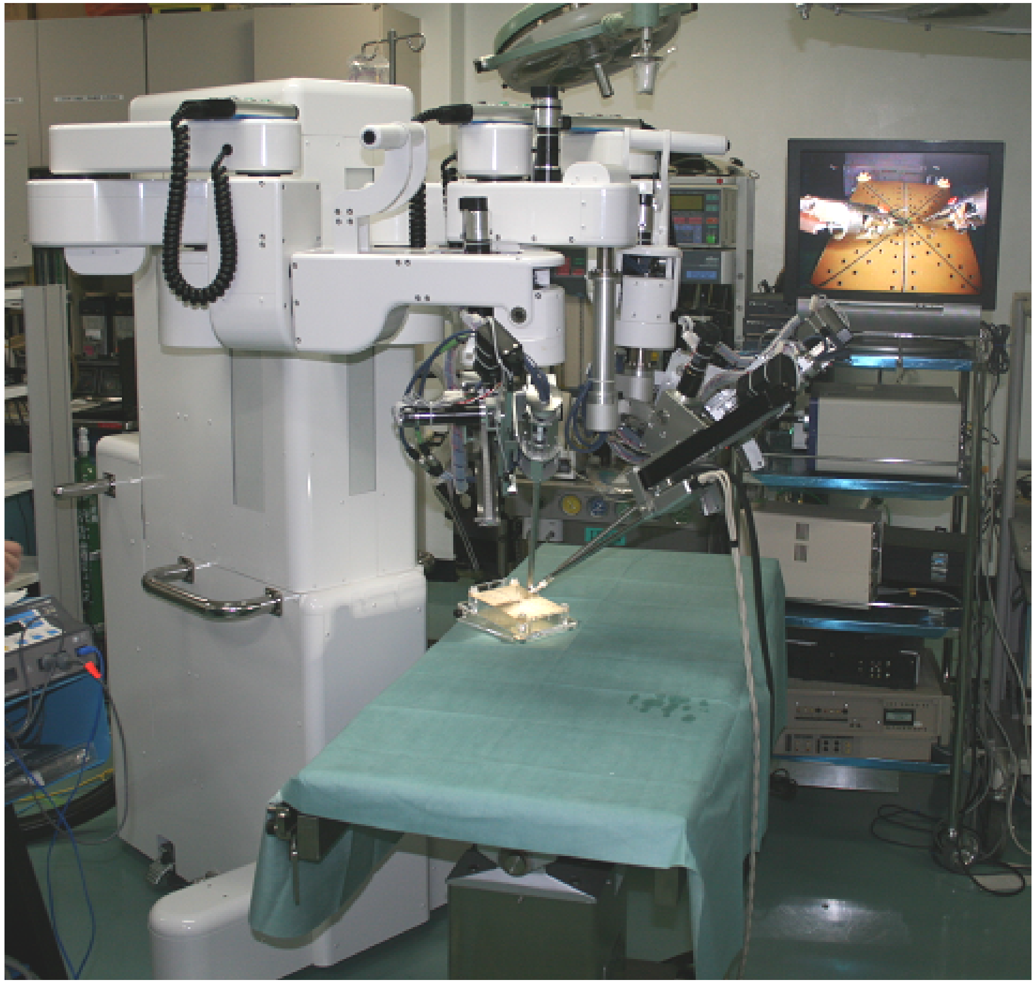

- Setup easiness was increased.

- Size (storing):
1,300 x 900 x 1,750 mm
- Weight: 630 kg
- Degrees of freedom: 33

- 2 forceps arms:
- D.o.f.: 13
- Arm length: 1,350 mm

- Endscope arm:
- D.o.f.: 7
- Arm length: 1,190 mm

Forceps arm

Preoperative rough positioning part: 6 d.o.f., fixed by electromagnetic brakes

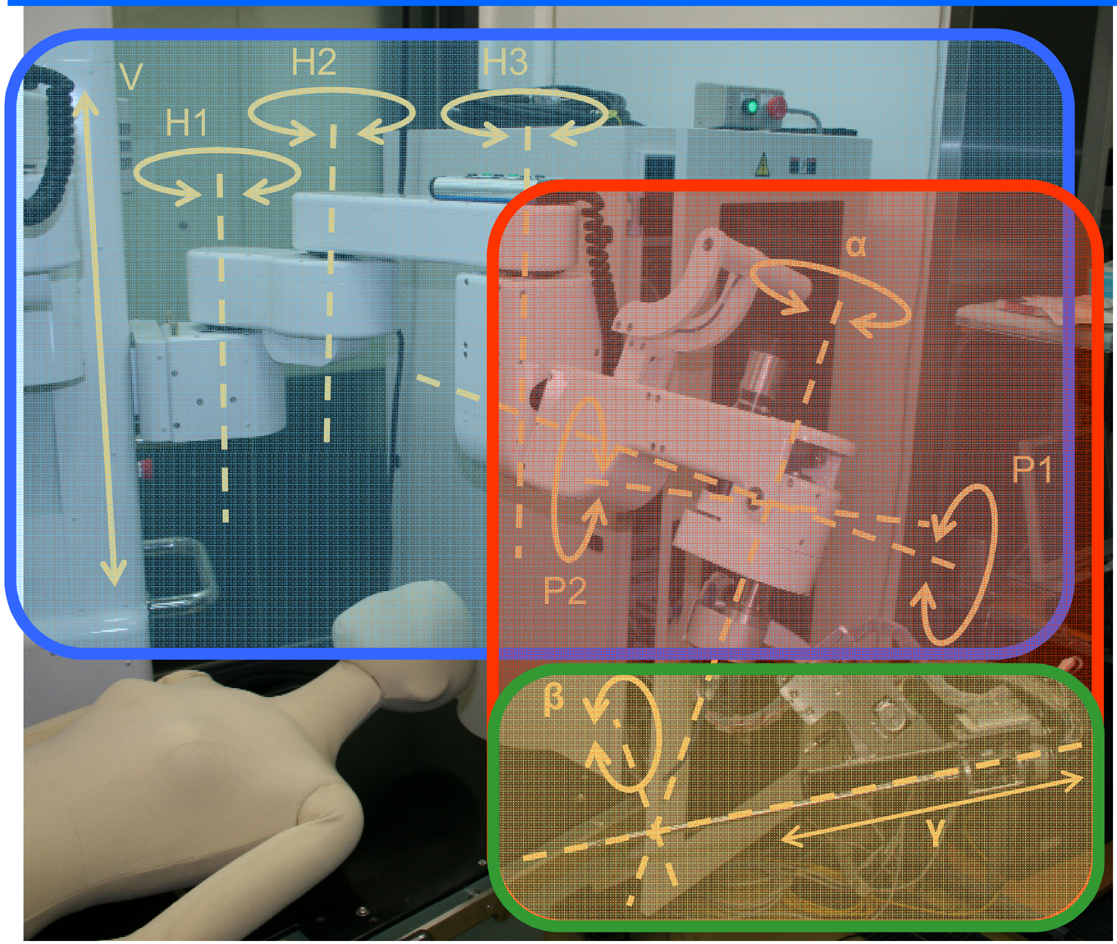

Surgical tool part: 4 d.o.f.

positioning part: 3 d.o.f.

Preoperative rough positioning part: 6 d.o.f.
- Vertical axis: V
- Horizontal axis: H1, H2, H3
- Posture axis: P1, P2

Intraoperative positioning part: 3 d.o.f.
- Rotational axis: α, β
- Translational axis: γ

Surgical tool part：Multi-axis bending forceps: 4 d.o.f.
- Rotaional axis: Roll
- Bending axis: δ, η
- Grasping axis: Pin

Redundant d.o.f. of the forceps arm

- Preoperative rough positioning part: 3 d.o.f.
- Redundant d.o.f.
- Intraoperative positioning part: 3 d.o.f.

- Posture change using the intraoperative positioning part increases the inserting direction range.
- The redundant axes avoid the interference with the other arms

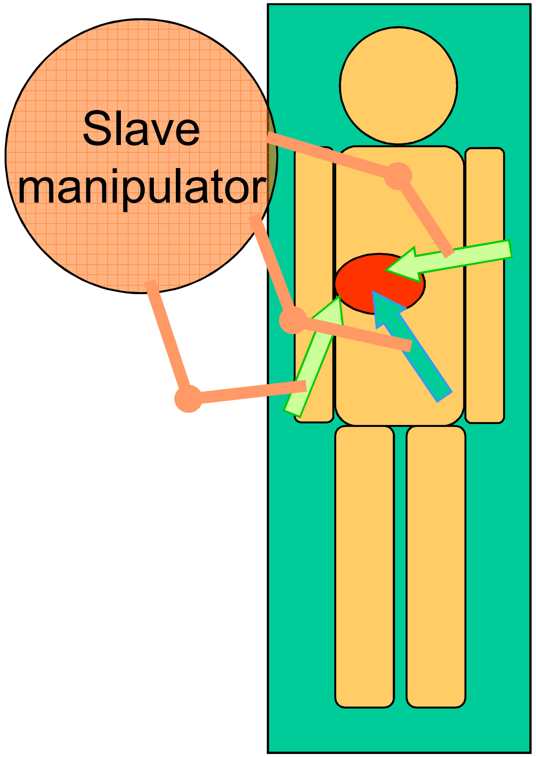

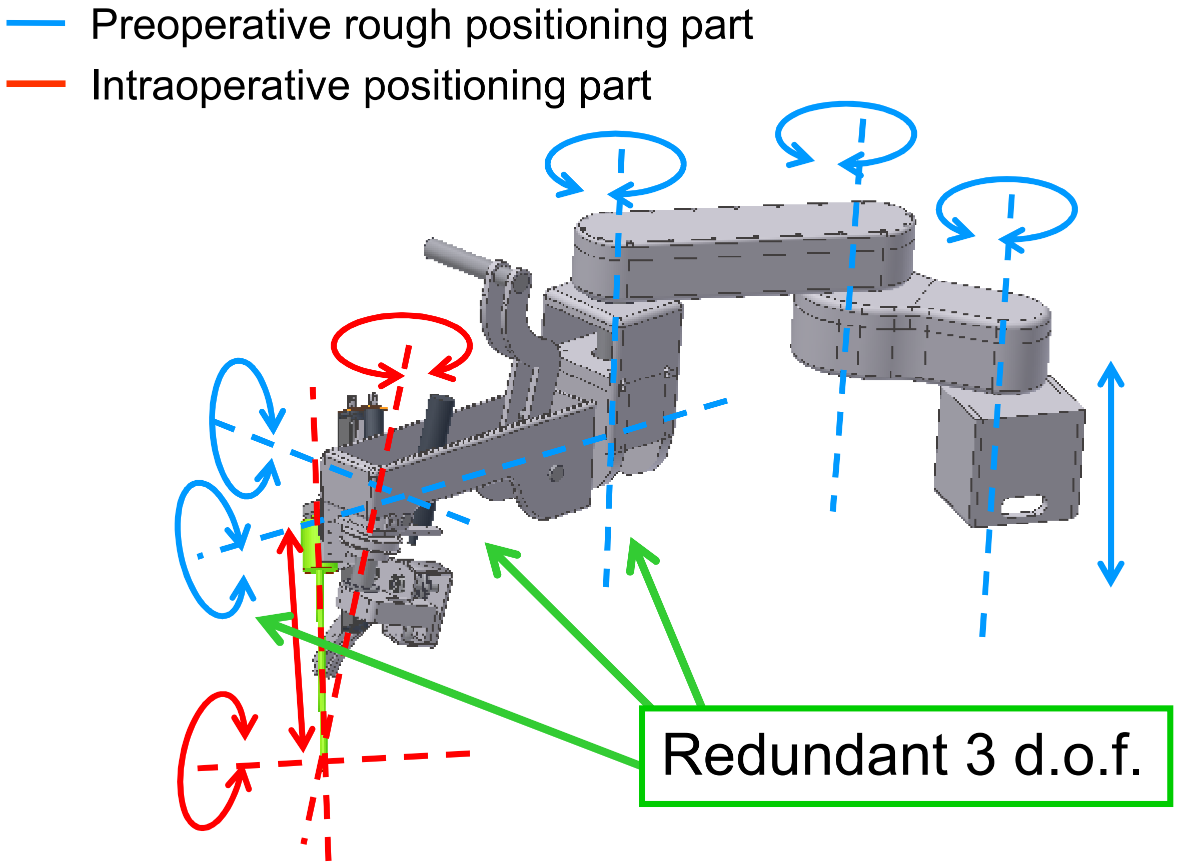

Endoscope arm

Preoperative rough positioning part: 4 d.o.f.: fixed by electromagnetic brakes

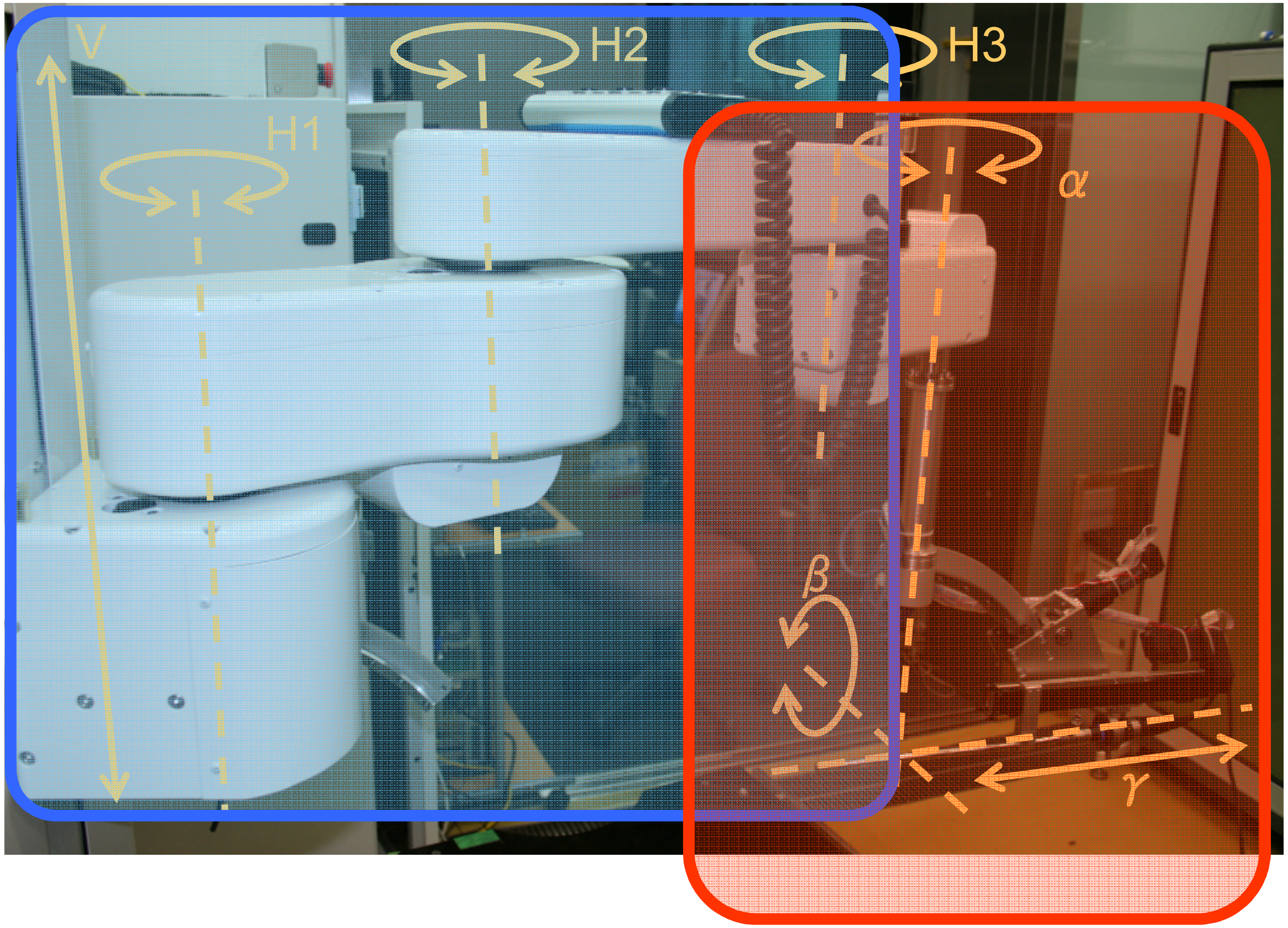

Preoperative rough positioning part: 4 d.o.f.
- Vertical axis: V
- Horizontal axis: H1, H2, H3

Intraoperative positioning part: 3 d.o.f.
- Rotational axis: α, β
- Translational axis: γ

Intraoperative positioning part: 3 d.o.f.

Redundant d.o.f. of the endoscope arm

- Preoperative rough positioning part: 3 d.o.f.
- Redundant d.o.f.
- Intraoperative positioning part: 3 d.o.f.

⇒

- Posture change using the intraoperative positioning part increases the inserting direction range.
- The redundant axes avoid the interference with the other arms

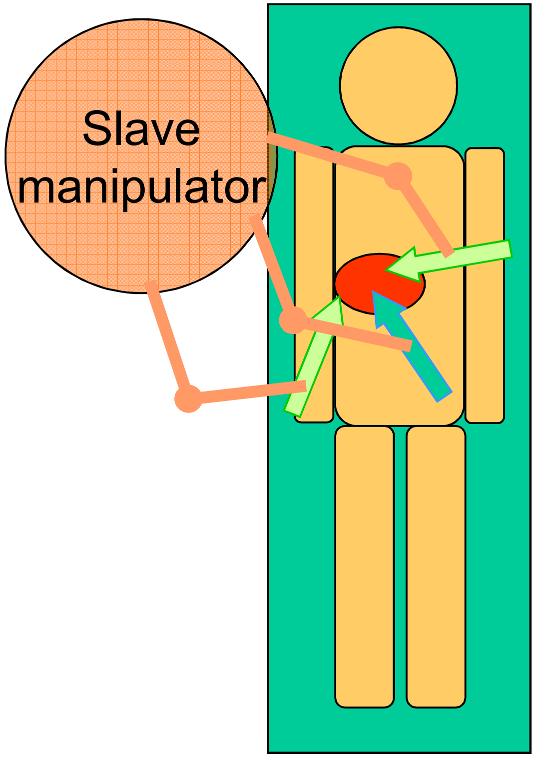

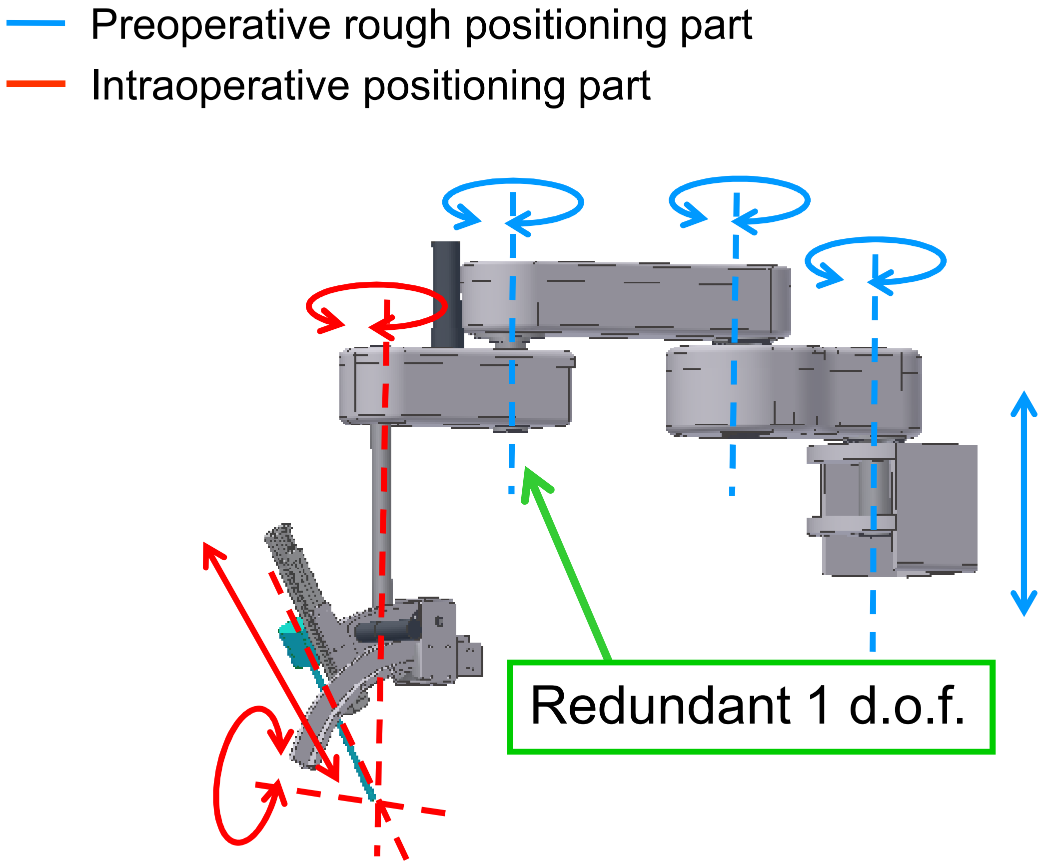

Trocar position comparison

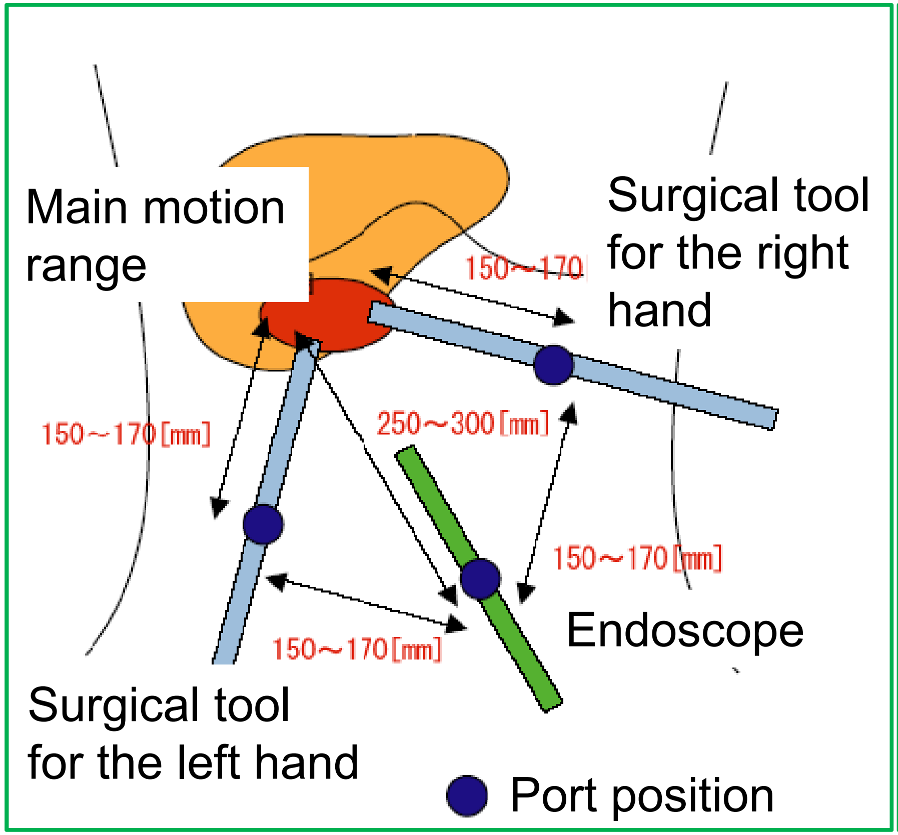

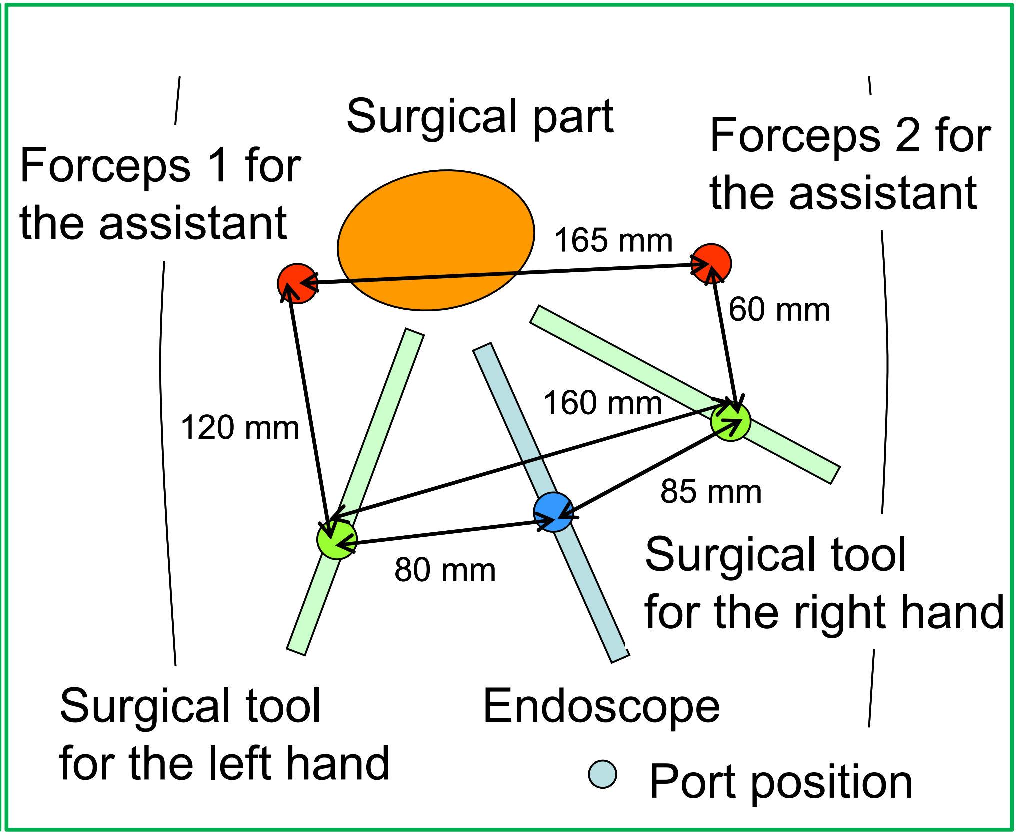

	Previous slave manipulator	Newly developed slave manipulator
Pig	50 kg	30 kg
Distance between the ports	150～170 mm	80～85 mm
Required time	40 min.	15 min.

Network configuration

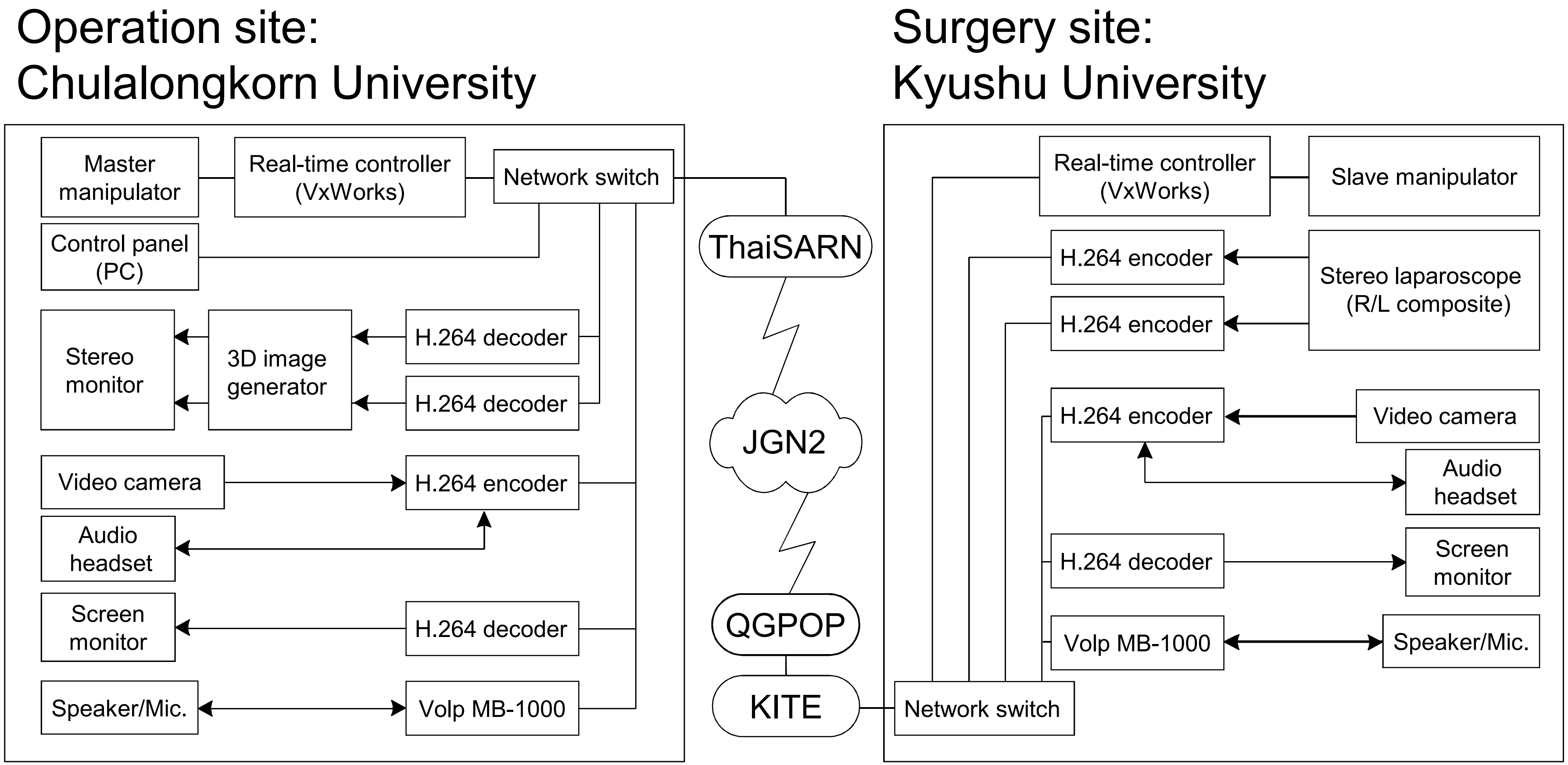

JGN2 : Japan Gigabit Network2 (30 Mbps was kept in the experiment)
ThaiSARN : Thai Social/Scientific Academic and Research Network
QGPOP : Kyushu GigaPoP Project
KITE : Kyushu University Integrated Information Transmission Environment

Laparoscopic image transmission

- Stereotype laparoscope (LS-101D: SHINKO OPTICAL CO., LTD.) was adopted in the experiment.
- Left and right images were transmitted independently.
- They were composed into the 3D image at the operation site.

CODEC system

- An extremely low latency CODEC named H.264 was adopted (WarpVision: NTT Resonant Inc.).
- Total time delay to encode and decode was approximately 80 ms.
- Necessary bandwidth is 3 Mbps/line for one way.

Bandwidth for information transmission

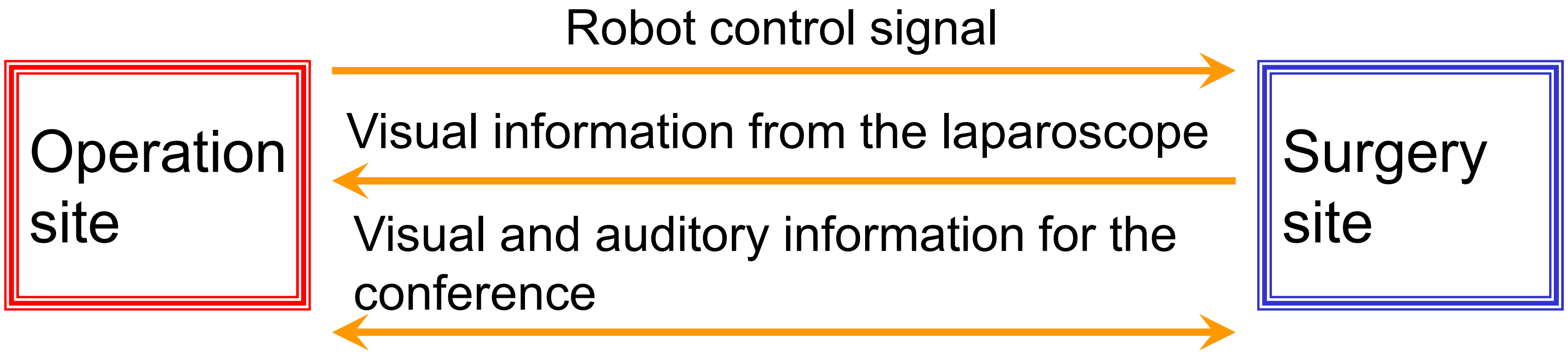

Transmitted data	Bandwidth
From operation site to surgery site:	
Robot control signal	6 kbps
Visual and auditory information for the conference	3 Mbps
From surgery site to operation site:	
Visual information from the laparoscope (L & R)	6 Mbps
Visual and auditory information for the conference	3 Mbps

Experimental result

Laparoscopic cholecystectomy and laparoscopic Nissen fundoplication were successfully performed on a pig using the developed system.

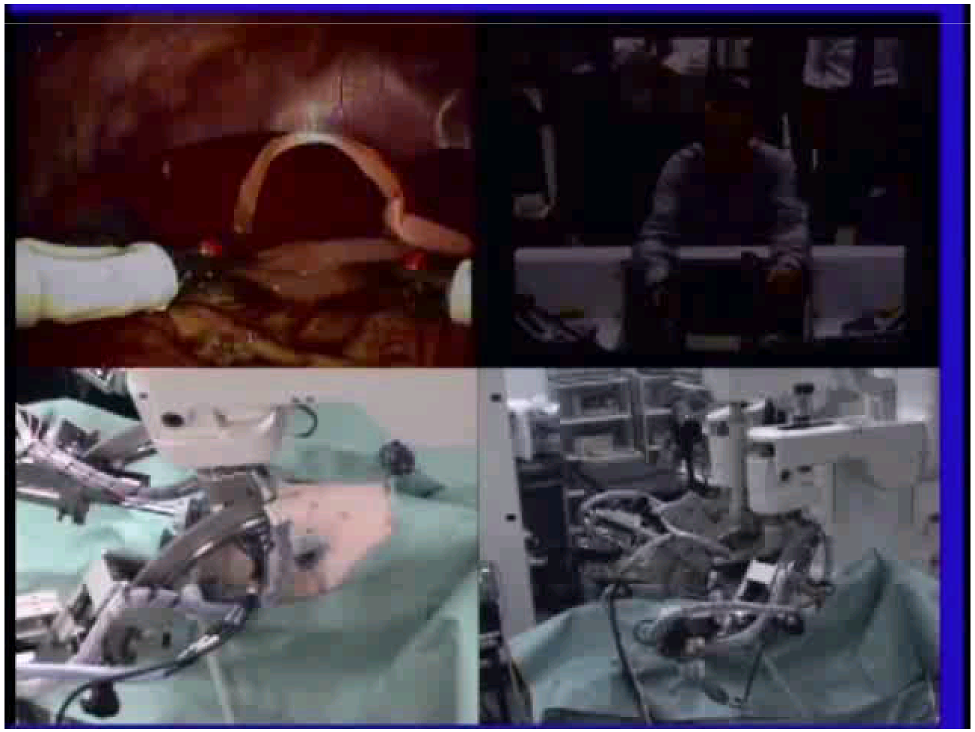

Cholecystectomy:
Total operation time: 84 min.

Time [min]	Contents
0	Start setup
15	Start removing gallbladder tube
52	Clip gallbladder tube, and start removing gallbladder
84	Take out gallbladder, and the end of operation

Nissen fundoplication:
Total operation time: 92 min.

Time [min]	Contents
0	Start setup
15	Start operation
92	End of operation

Time delay for transmitting the control signal

One way transmission time delay for the control signal was 57.1 ms.

Operation site – Surgery site	Time delay
Tokyo – Shizuoka (150km) by ISDN(2B+D)	49.9 ms
Tokyo – Shizuoka by ISDN(23B+D)	17.8 ms
Seoul – Fukuoka(540km) by APII	6.5 ms
Bangkok – Fukuoka (5,400km) by JGN2	62.4 ms
Bangkok – Fukuoka by JGN2	57.1 ms

Time delay for transmitting the visual information

One way transmission time delay for the visual information was 151.2 ms.

Operation site – Surgery site	Time delay
Tokyo – Shizuoka (150km) by ISDN(2B+D)	338.0 ms
Tokyo – Shizuoka by ISDN(23B+D)	392.5 ms
Seoul – Fukuoka (540km) by APII	435.5 ms
Bangkok – Fukuoka (5,400km) by JGN2 Normal	370.0 ms
Bangkok – Fukuoka by JGN2 MPG2 Low latency	270.0 ms
Bangkok – Fukuoka by JGN2 H.264 Low latency	151.2 ms

Time delays that the operator feels

(Sensible time delay for the operator: 278.3 ms)
= (Communication period between the master and slave manipulators: 20.0 ms)
+ (Time delay for transmitting the position information: 57.1 ms)
+ (Mechanical response time of the slave manipulator: 50.0 ms)
+ (Time delay of the image transmission: 151.2 ms)

Operation site – Surgery site	Time delay
Tokyo – Shizuoka (150km) by ISDN(2B+D)	537.9 ms
Tokyo – Shizuoka by ISDN(23B+D)	592.4 ms
Seoul – Fukuoka(540km)	592.0 ms
Bangkok – Fukuoka (5,400km) MPG2 Low latency	540.0 ms
Bangkok – Fukuoka H.264 Low latency	278.3 ms

Relation between the required time for positioning and the time delay

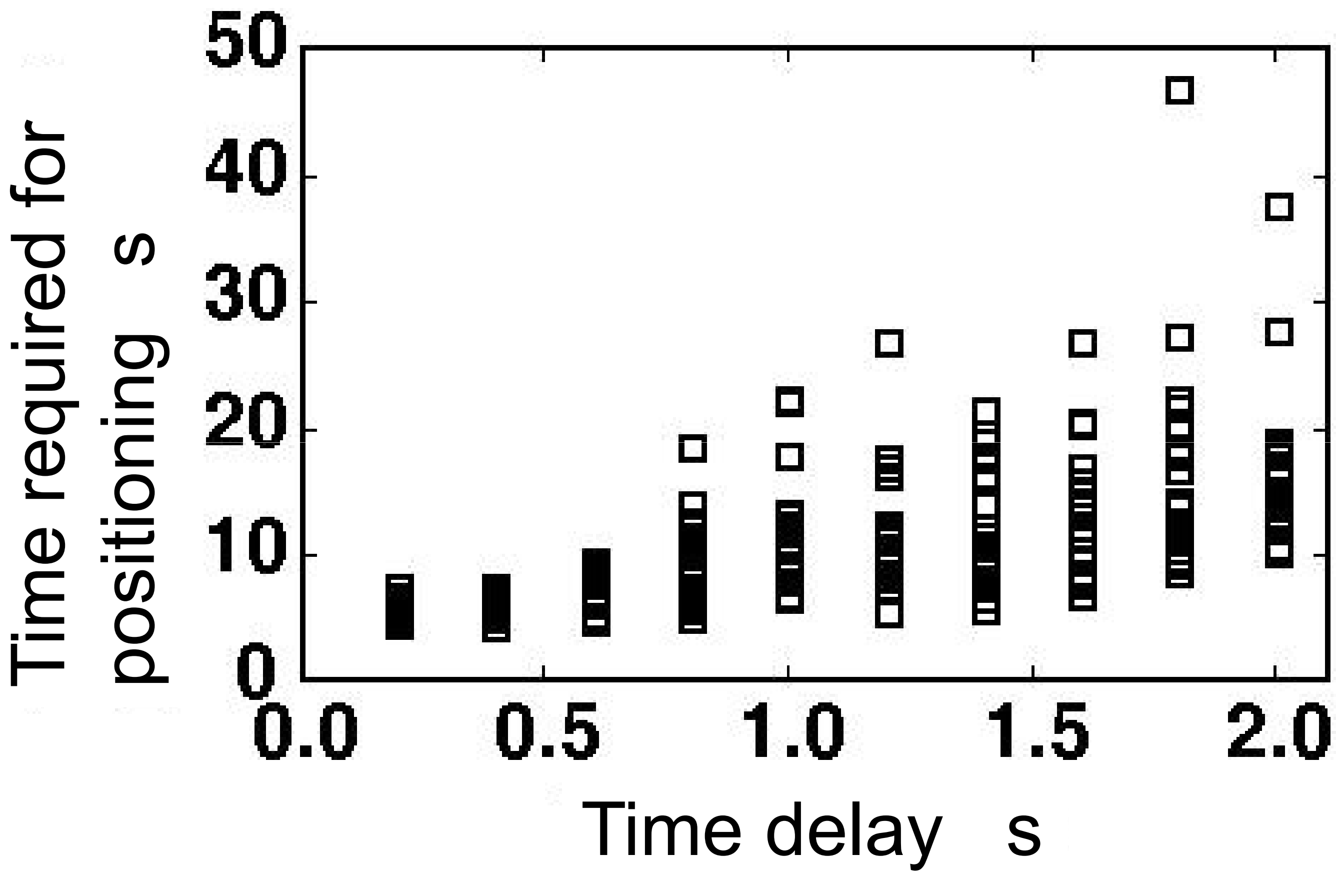

Comparison of the visual information quality

<u>Fukuoka-Bangkok</u>
MPG2 low latency
Time delay 270 ms

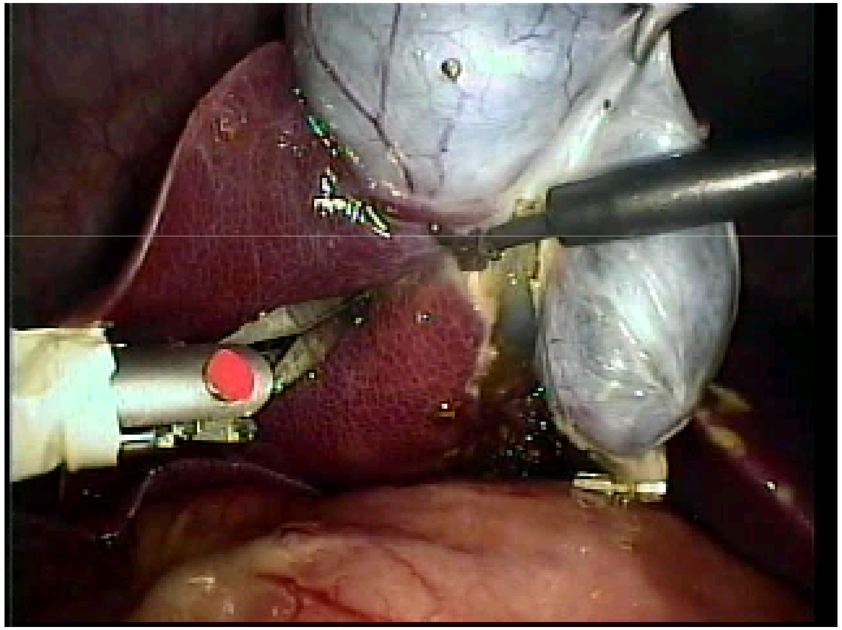

Block noise was detected.
(January, 2006)

<u>Fukuoka-Bangkok</u>
H.264 low latency
Time delay 151.2 ms

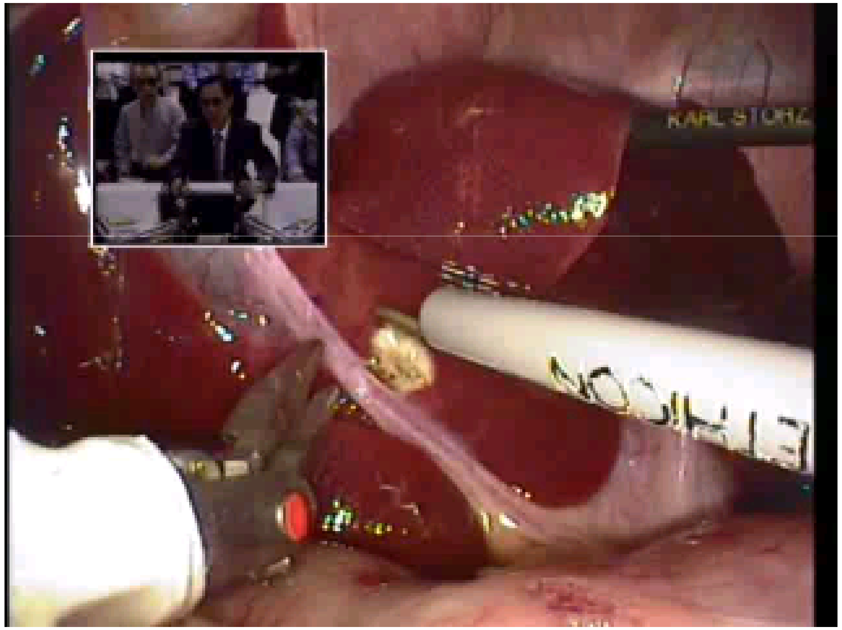

Block noise was not detected.
(March, 2008)

Medical system in the future

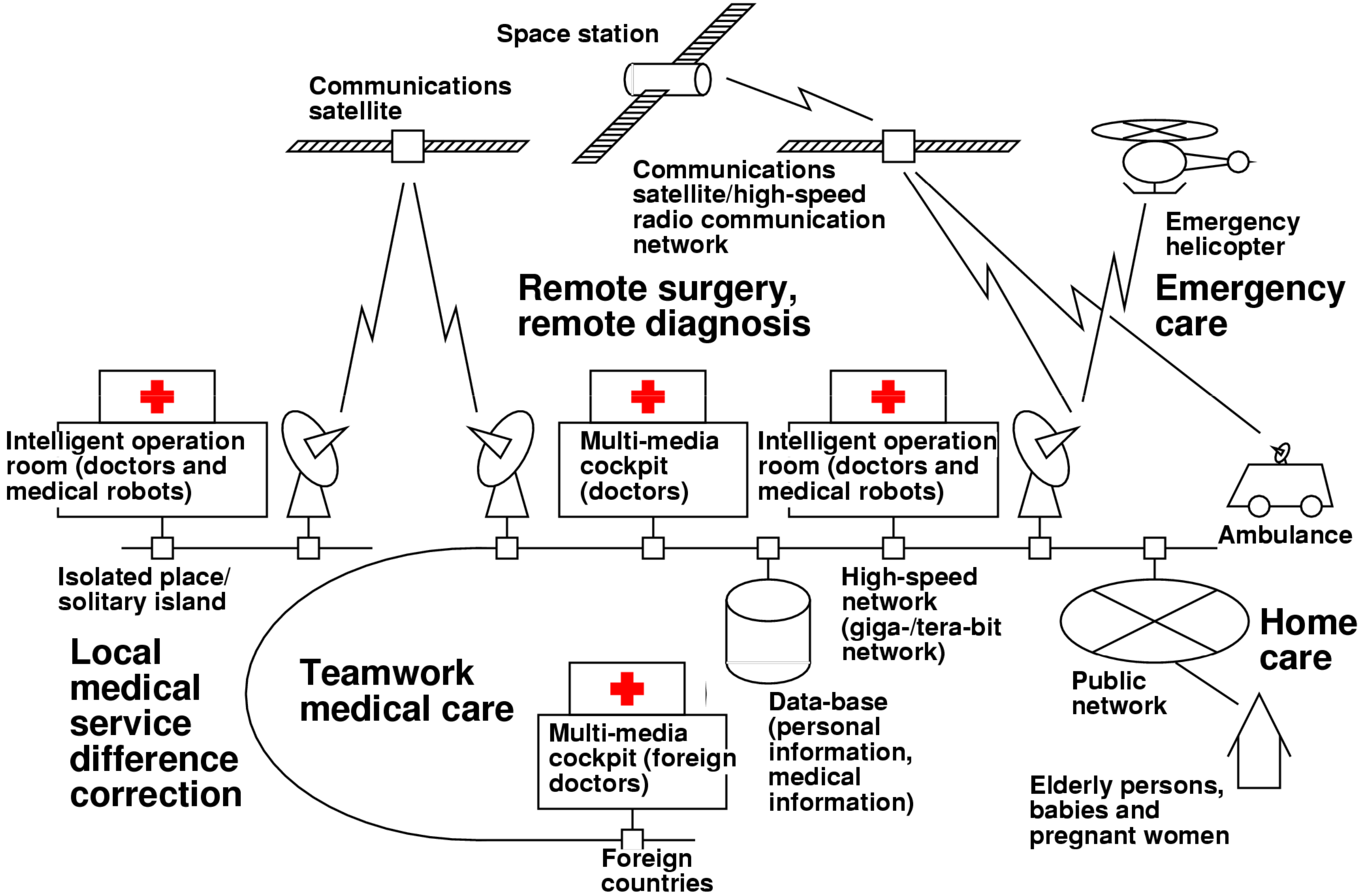

Conclusions

1. A slave manipulator for the abdominal surgery was developed. Setup easiness was increased. Distance between trocars was reduced.
2. The authors conducted the telesurgery experiment between Japan and Thailand using a newly developed robot.
3. A laparoscopic cholecystectomy and a laparoscopic Nissen fundoplication were successfully performed on a pig.
4. Each operation time was approximately 90 min.
5. Time delay for visual information transmission was reduced to 151.2 ms by adopting H.264 low latency CODEC. Block noise was not detected.
6. Sensible time delay in the experiment was 278.3 ms (< 300 ms).

Introduction

High Intensity Focused Ultrasound（HIFU）

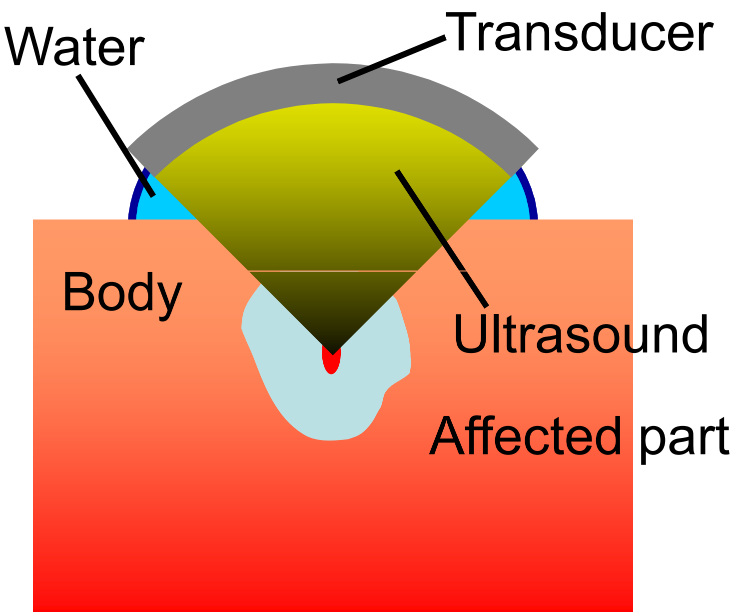

High Intensity
Focused Ultrasound

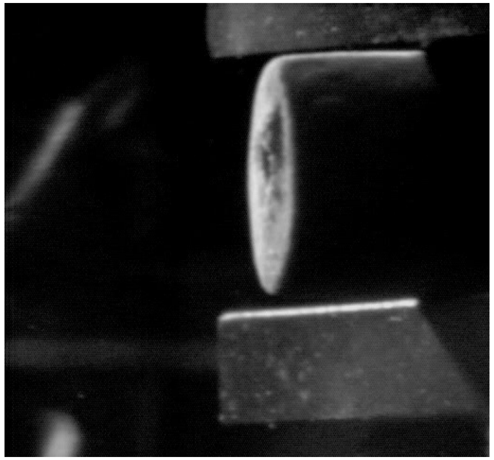

Y. Matsumoto, et. al.

Destruction of stone

JC HIFU System (in China)

Clinical use

Stone destruction by CCL (cavitation control lithotripsy) method

PRF (pulse rate frequency): 20 Hz

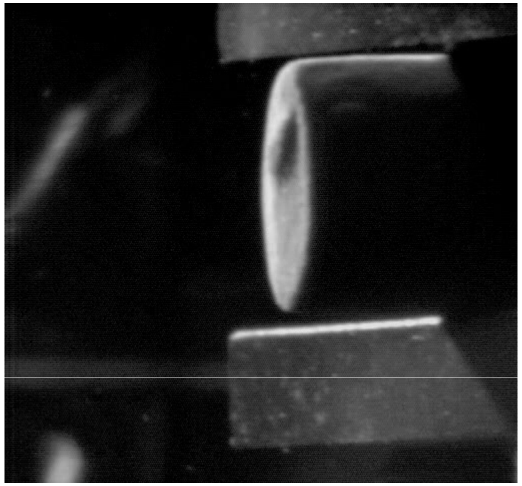

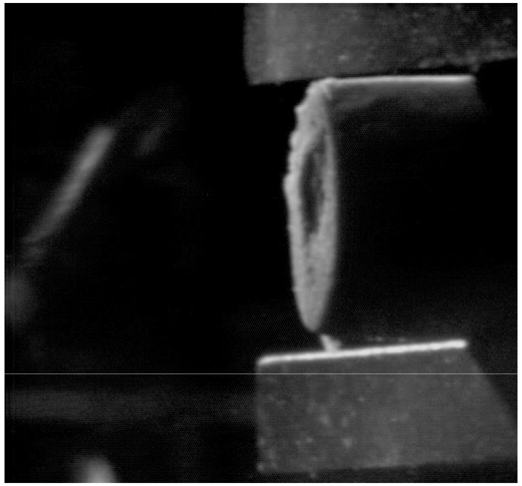

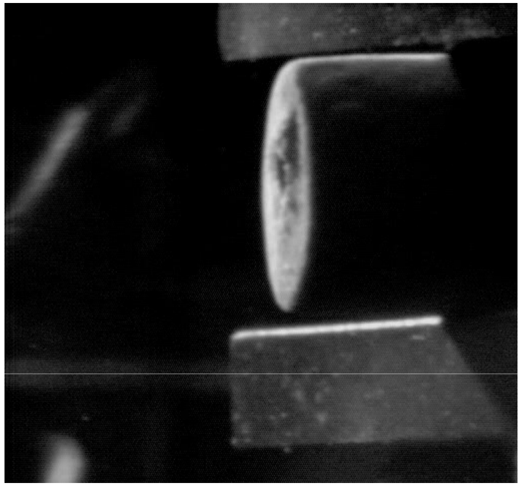

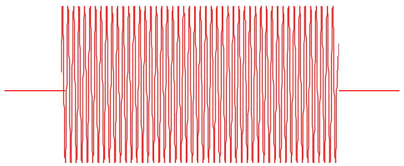

High freq.：3.8 MHz
200 waves

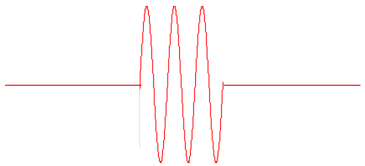

Low freq.：553 kHz
3 waves

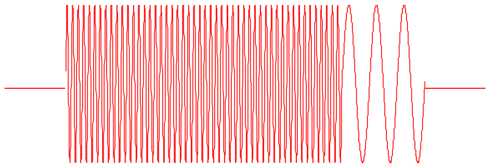

High freq.＋Low freq.

Stones is destroyed

⇒Required to irradiate HIFU to a kidney stone continuously

Problems

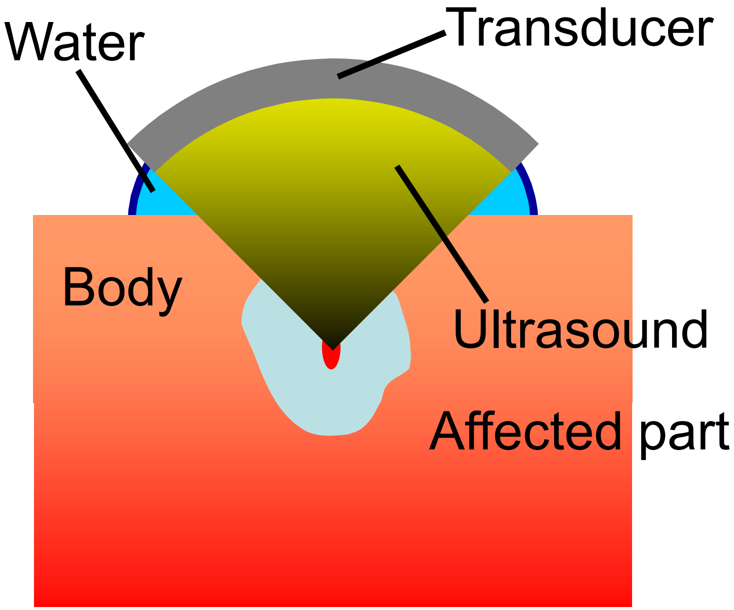

High Intensity Focused Ultrasound

Problem of HIFU

Motion of the affected part by the respiration

Solution

Compensation of the motion of the affected part should be required.

Objective

Establish a control method to compensate for the motion of the affected part by respiration

Required accuracy: 1mm

System configuration

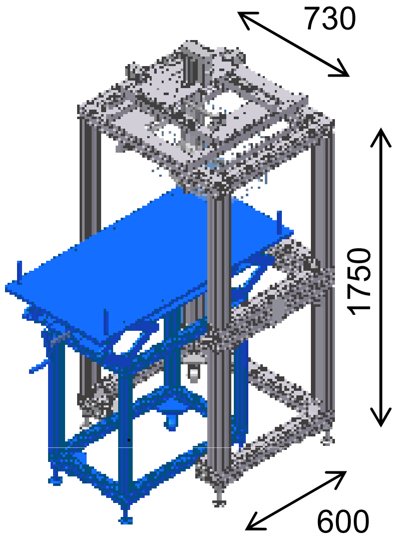

(a) Isometric view

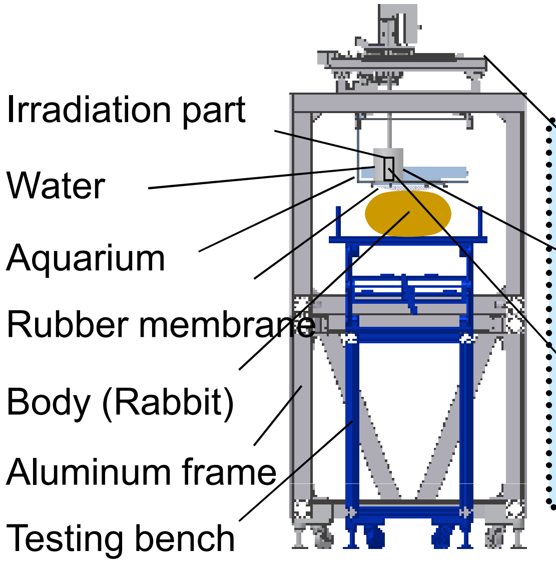

(b) Front view

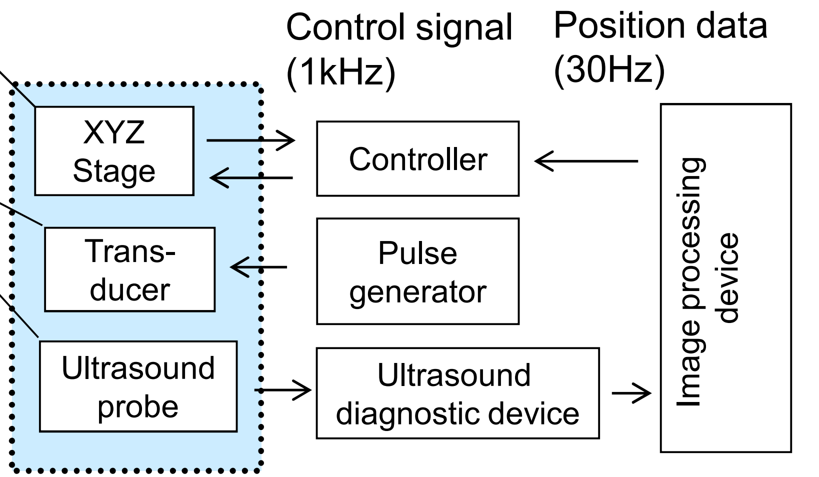

Stone motion tracking capability

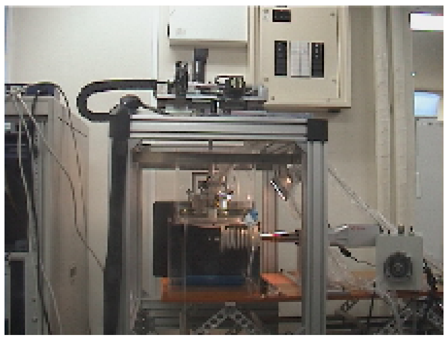

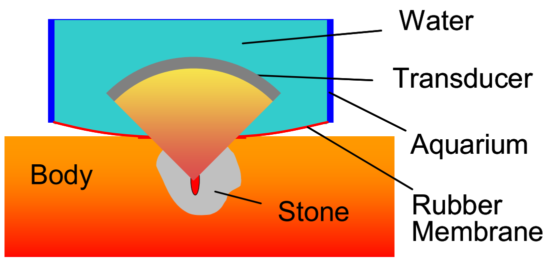

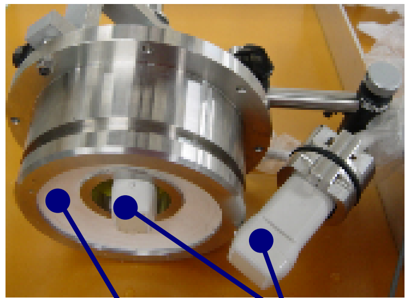

Transducer Probes

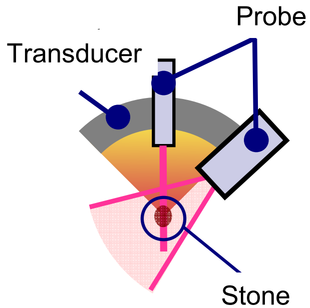

Water to secure ultrasound path to the affected part

2 ultrasound probes for 3 dimensional position data

Interference avoidance between HIFU and ultrasound probe

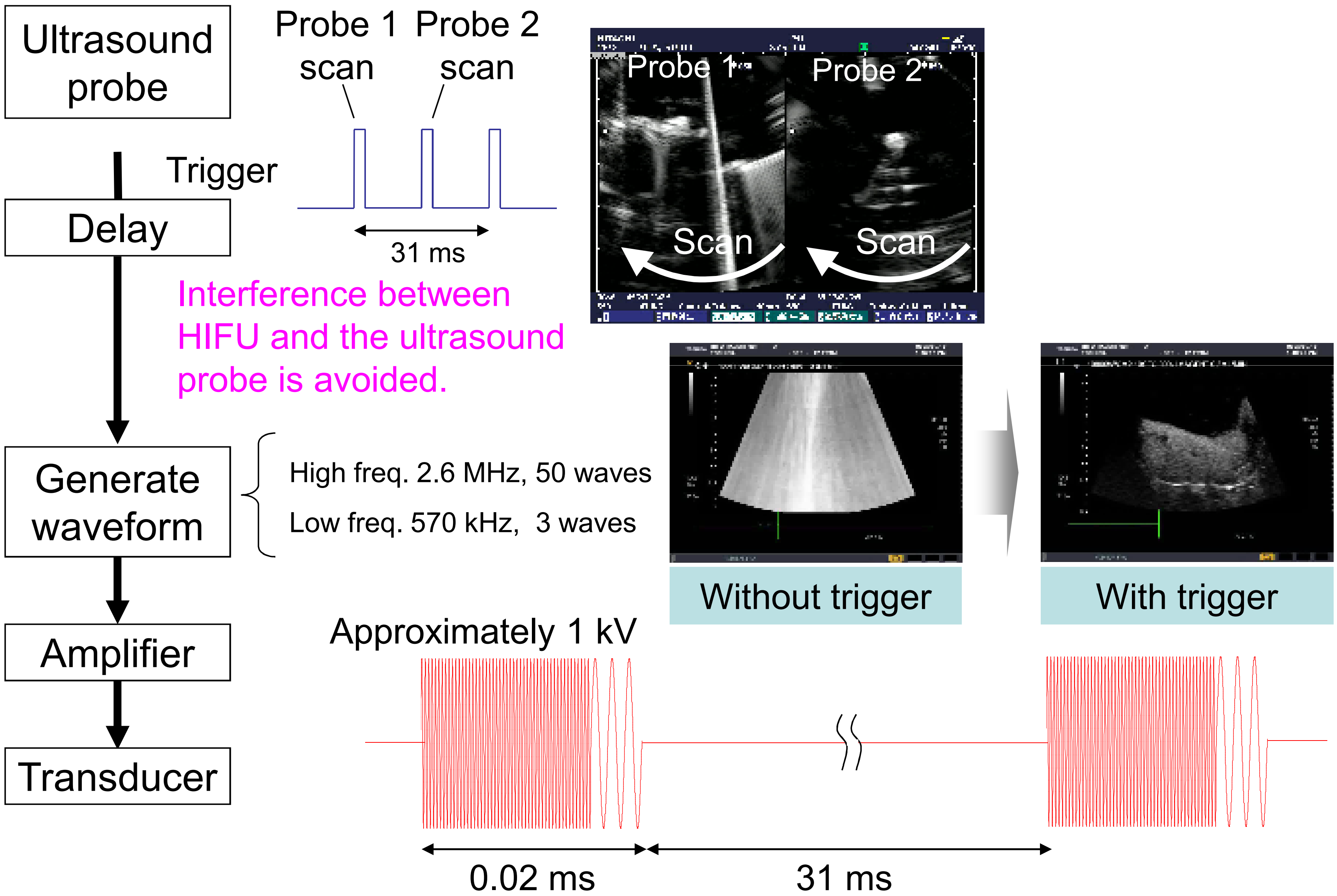

Constructed system

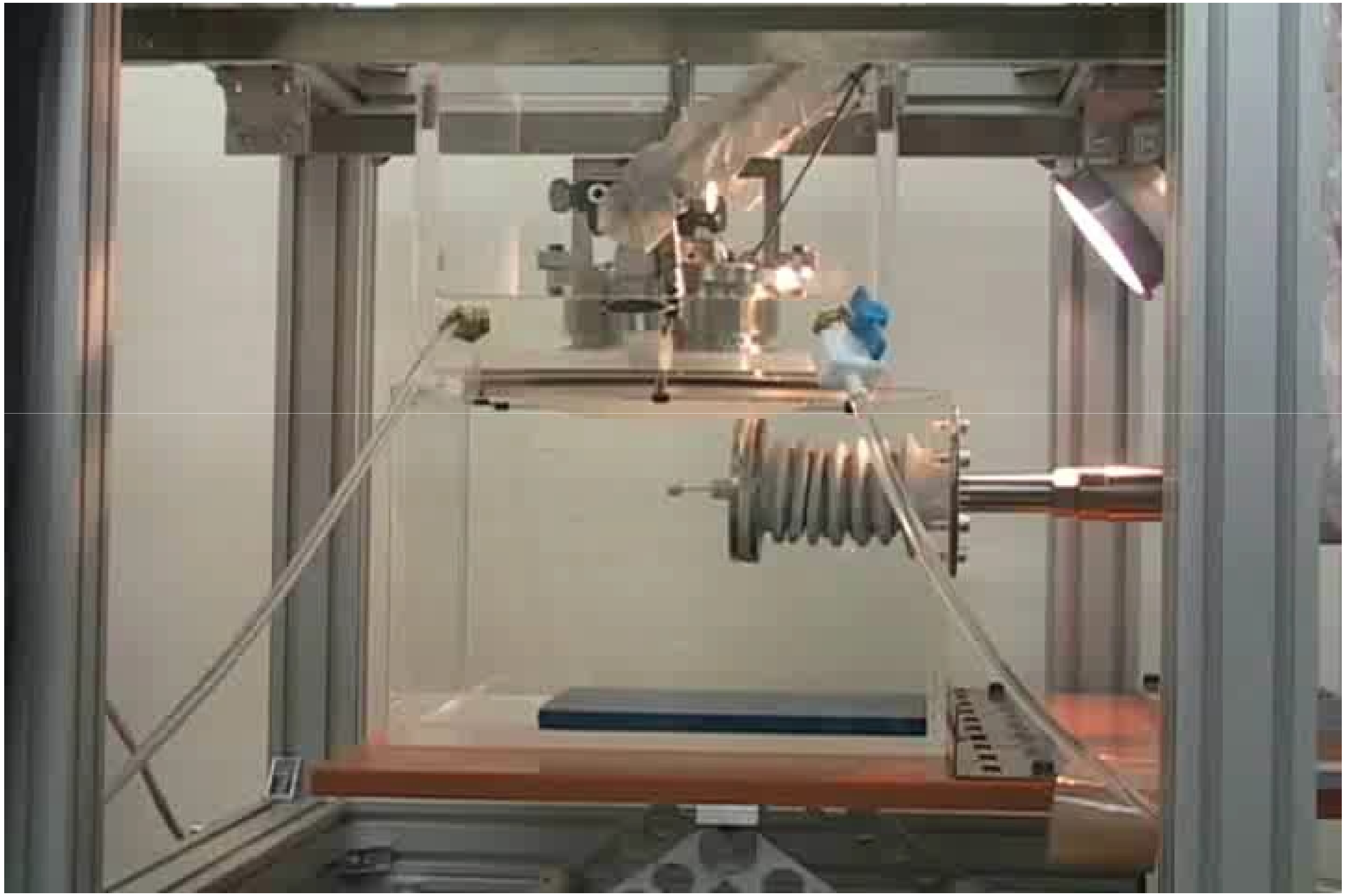

Problem while tracking a kidney stone on the ultrasound image

Without bubble

Tracking failure because of bubble

Tracking error increase

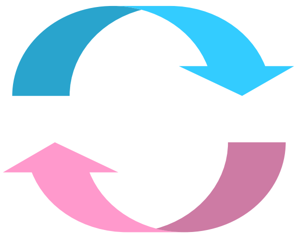

Image quality decreases because of the tracking errors, bubbles, and mechanical oscillations.

Automatic/semi-automatic extraction of kidney stone

Kidney store has high Intensity on the ultrasound image, due to the higher acoustic impedance compared to other tissues.

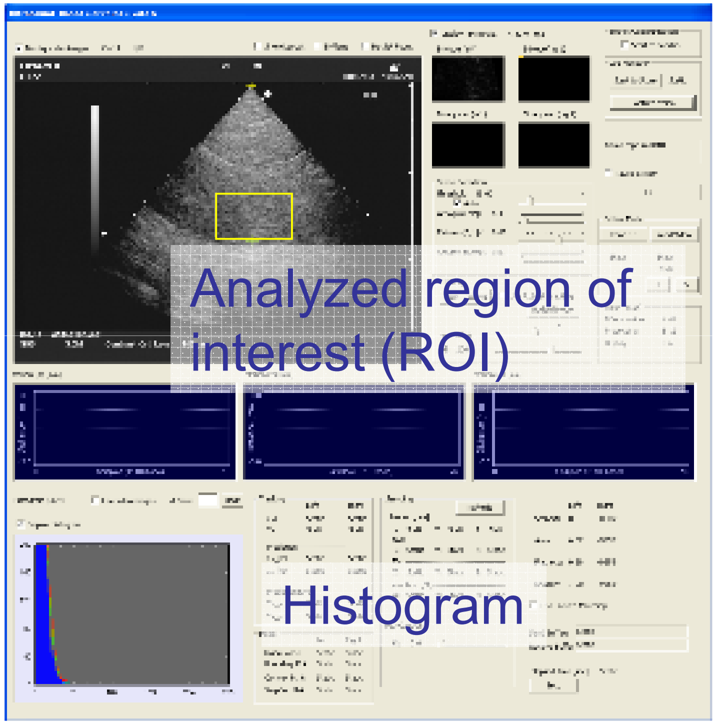

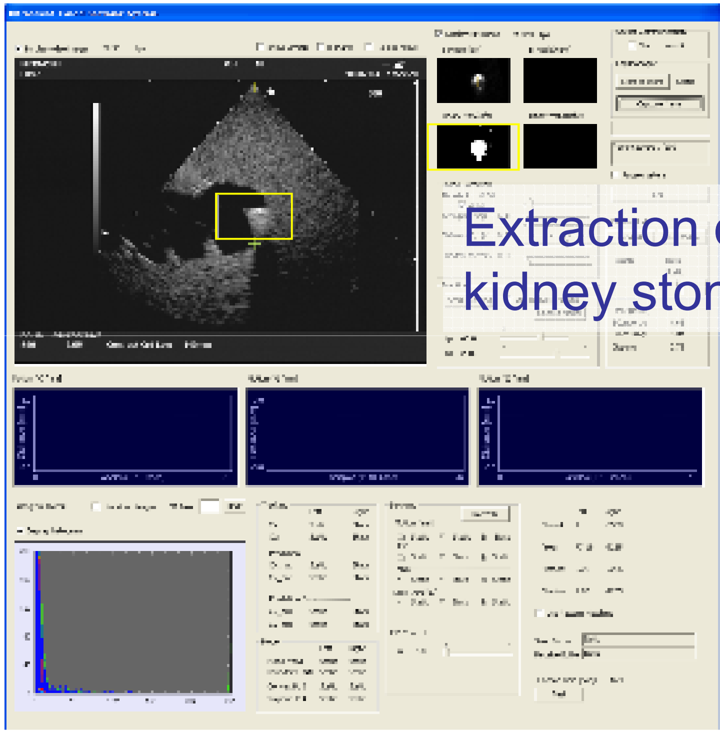

High acoustic impedance compared to the neighboring tissues

Table Reflection coefficients in human abdomen

$R = \frac{Z_2 - Z_1}{Z_2 + Z_1}$	Blood	Fat	Muscle	Kidney	Water	Renal calculi
Blood	0	0.08	0.024	0	0.032	0.325 to 0.601
Fat		0	0.104	0.08	0.0482	0.395 to 0.650
Muscle			0	0.024	0.056	0.303 to 0.586
Kidney				0	0.0318	0.325 to 0.601
Water					0	0.353 to 0.621
Renal calculi						0

Automatic extraction of kidney stone using intensity histogram

Threshold between kidney stones and tissues is determined using Rayleigh Curve (model of typical background) at the input ultrasound image

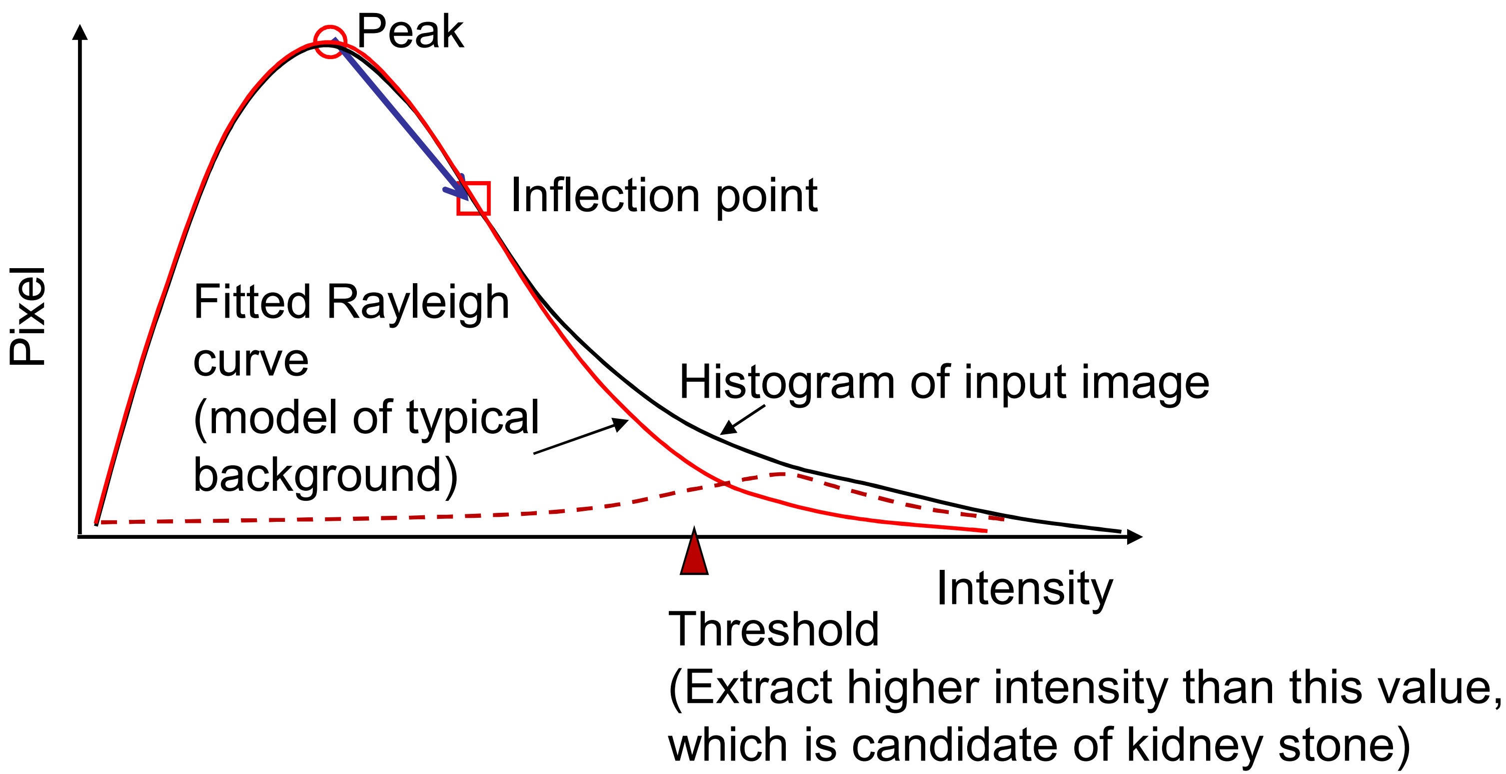

Generalized Rayleigh Curve: $f(x \mid \sigma, S, x_0) = \frac{x - x_0}{\sigma^2} \exp \frac{-(x - x_0)^2}{2S^2\sigma^2}$

Automatic extraction of kidney stone using acoustic shadow

Find a kidney stone by acoustic shadow (radiated shadow) behind the kidney stone candidates

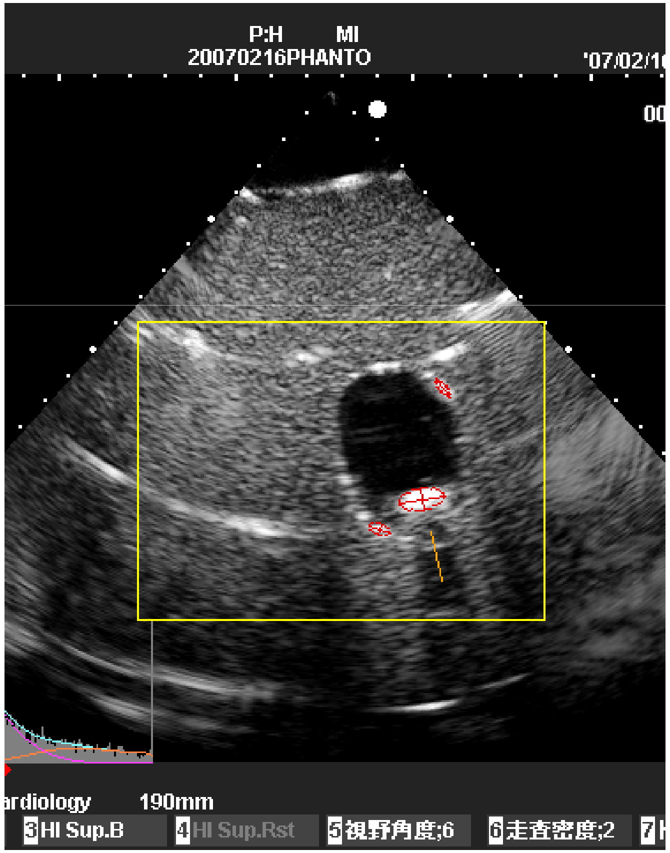

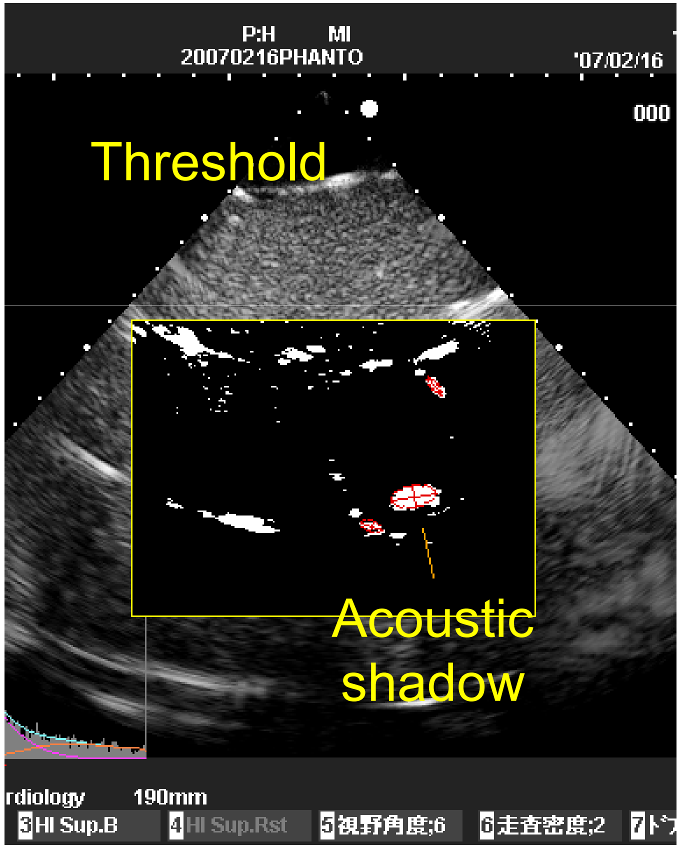

Robust motion track by shape information

Stone motion is tracked robustly using the shape information even if the stone is partially contaminated by bubbles.

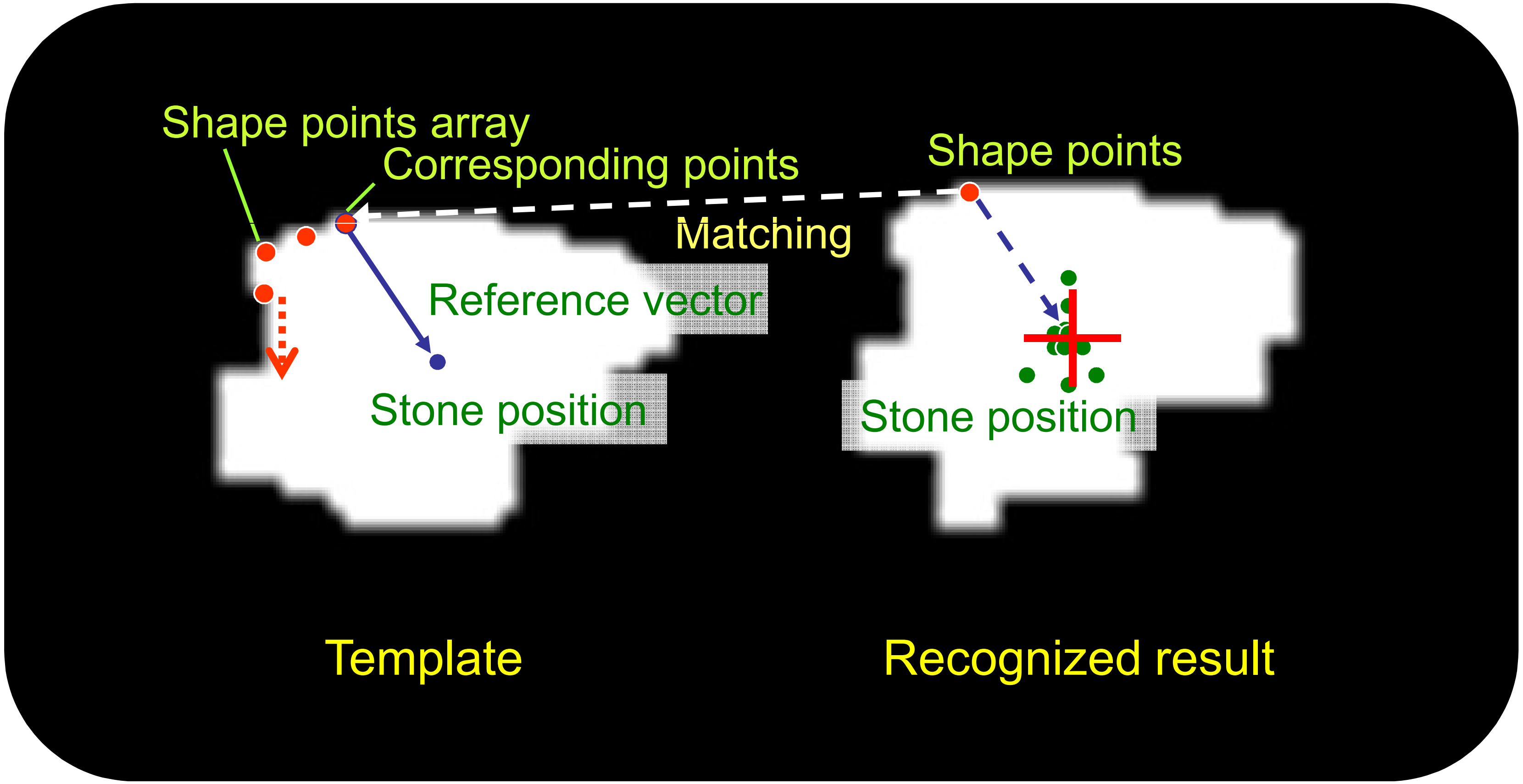

Characteristics of kidney motion

Kidney motion

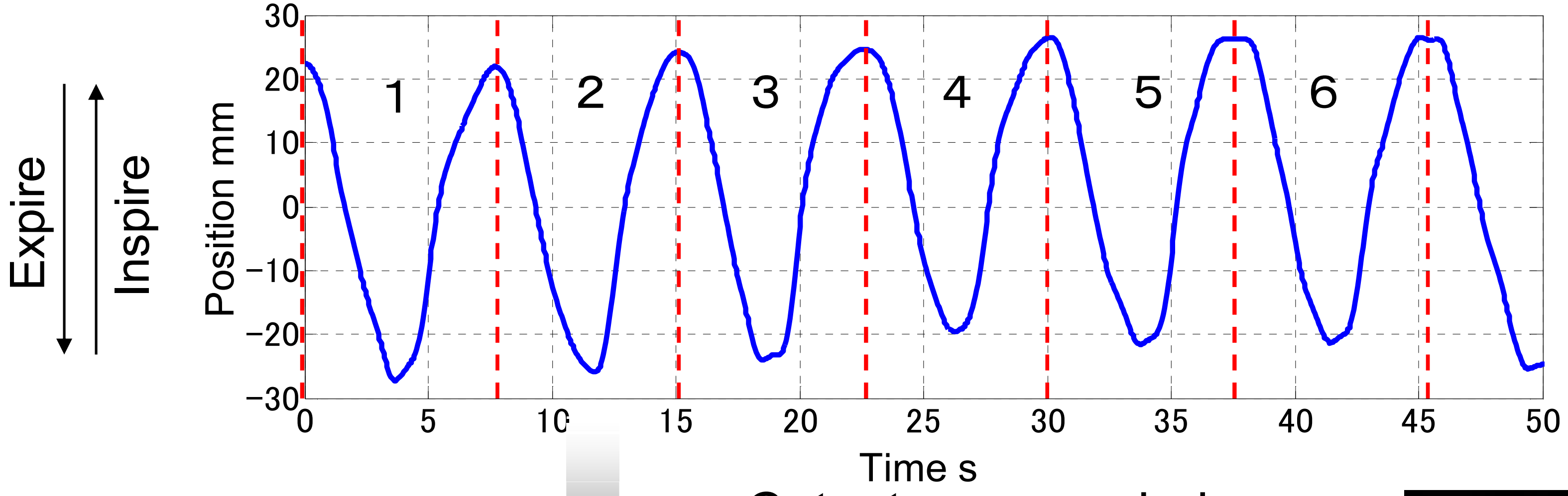

Cut at every period

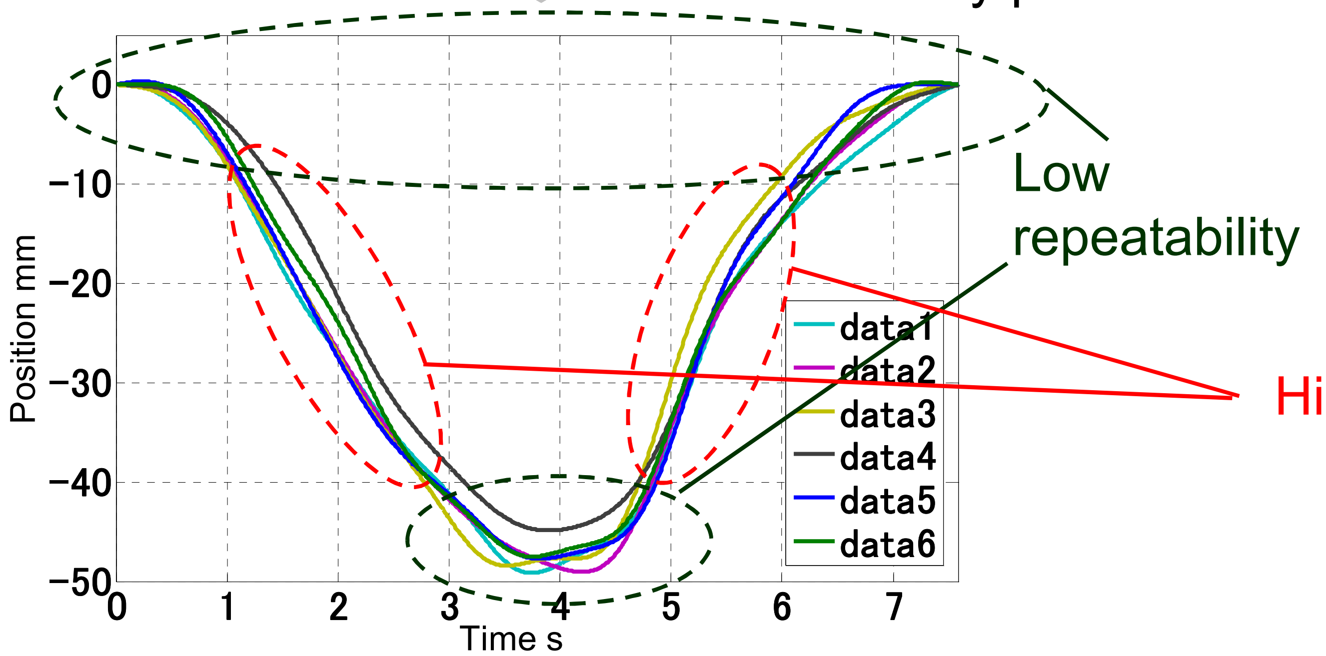

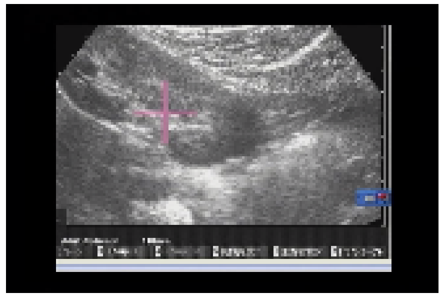

Kidney motion

Servoing performance enhancement using periodical characteristics of kidney motion

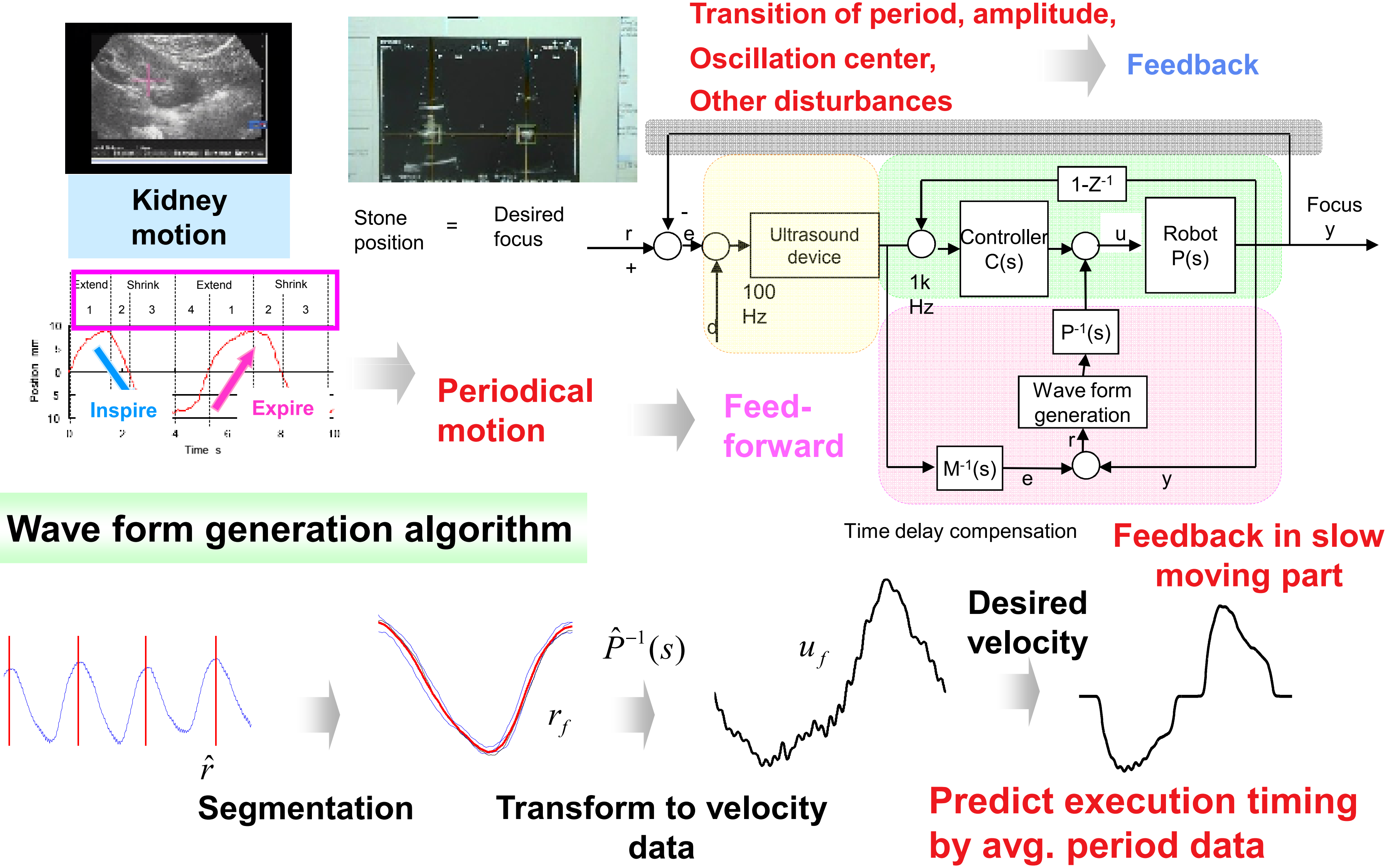

Servoing performance enhancement by semi-periodical kidney motion

Input and output of respiratory kidney motion

Servoing error

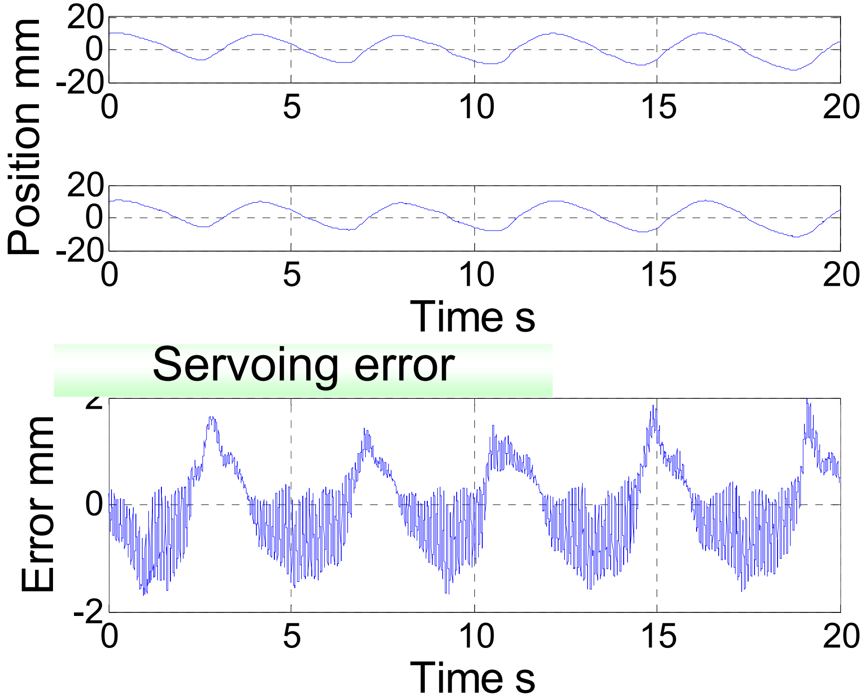

Feedback (FB)

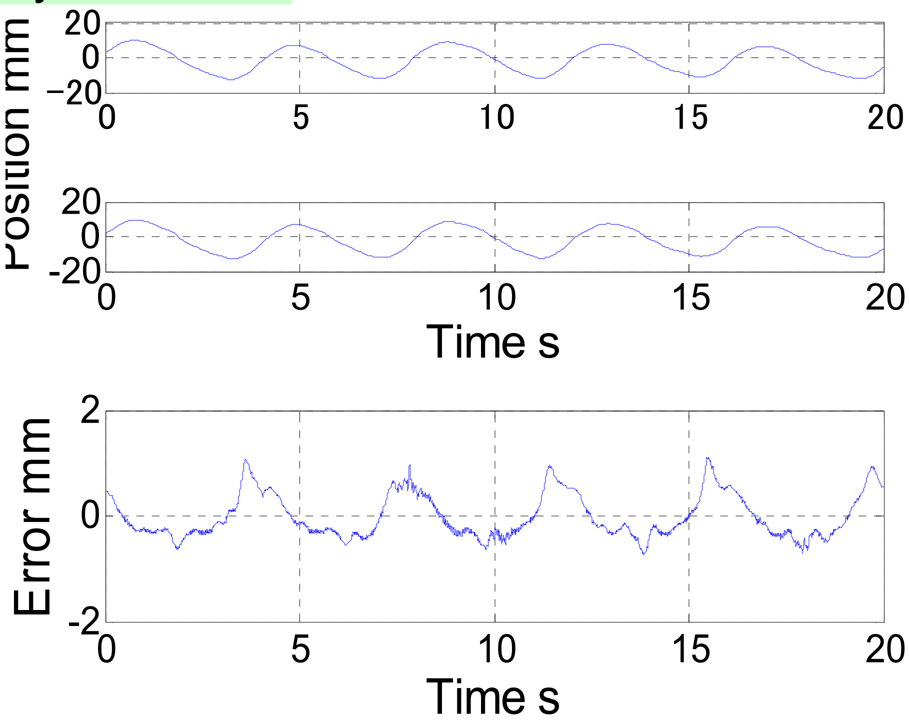

Proposed method

Evaluation	FB	FB+FF
Max. error [mm]	1.99	1.15
Avg. error [mm]	0.67	0.36
Standard deviation [mm]	0.42	0.21

- Average error: 0.36 mm
- Oscillation was suppressed.

Ex vivo servoing and HIFU irradiation

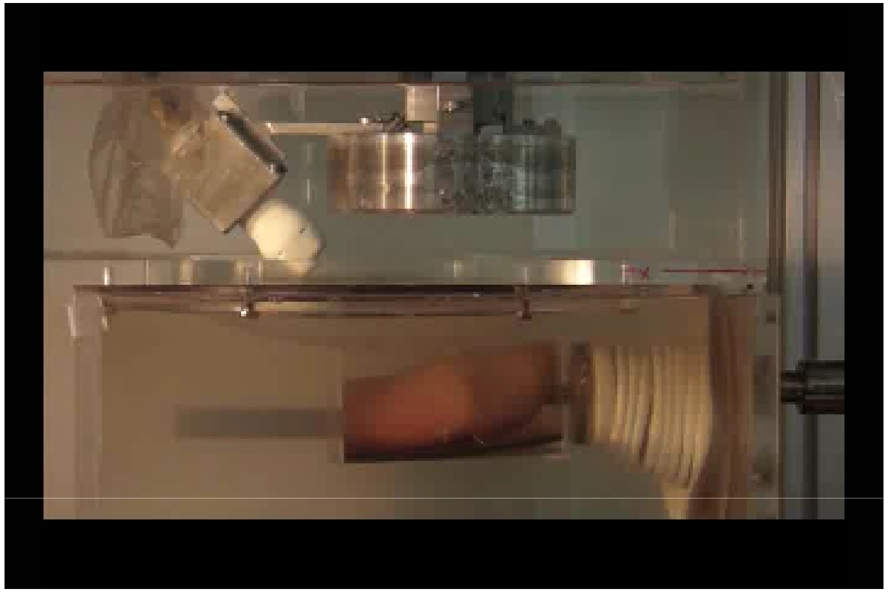

Experimental setup

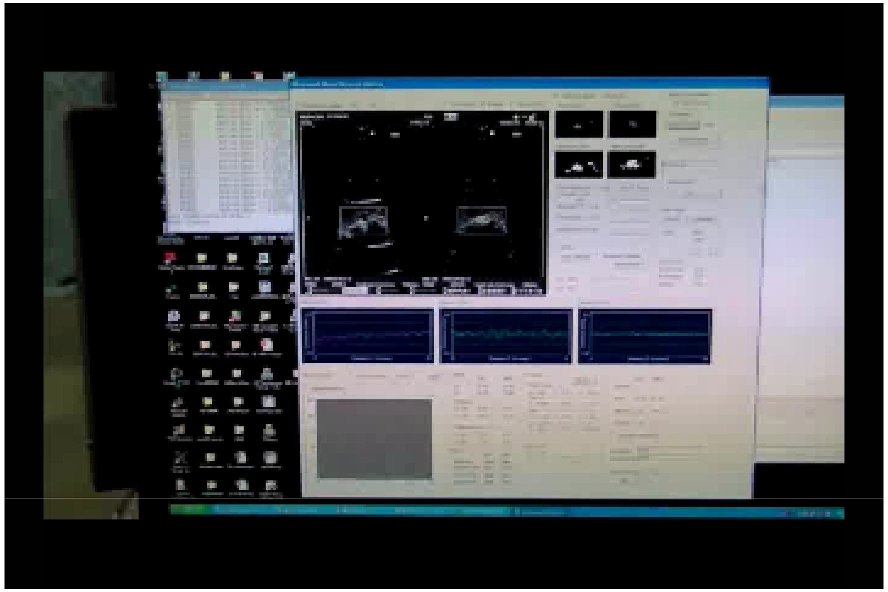

Ultrasound image

Model stone was set in the swine kidney

Ex vivo servoing was realized.